Cladding modes of optical fibers: properties and applications

2006 Phys.-Usp. 49 167

(http://iopscience.iop.org/1063-7869/49/2/R02)

Physics – Uspekhi **49** (2) 167 – 191 (2006)

INSTRUMENTS AND METHODS OF INVESTIGATION PACS numbers: **42.25. – p**, 42.79.Gn, **42.81. – i**

Cladding modes of optical fibers: properties and applications

O V Ivanov, S A Nikitov, Yu V Gulyaev

DOI: 10.1070/PU2006v049n02ABEH005784

Contents

Abstract. One of the new methods of fiber optics uses cladding modes for controlling propagation of radiation in optical fibers. This paper reviews the results of studies on the propagation, excitation, and interaction of cladding modes in optical fibers. The resonance between core and cladding modes excited by means of fiber Bragg gratings, including tilted ones, is analyzed. Propagation of cladding modes in microstructured fibers is considered. The most frequently used method of exciting cladding modes is described, based on the application of long-period fiber gratings. Examples are presented of long-period gratings used as sensors and gain equalizers for fiber amplifiers, as well as devices for coupling light into and out of optical fibers.

1. Introduction

The development of fiber-optics technology has become an important part of the revolution in telecommunications. Recently, much progress has been achieved in the development of fiber amplifiers, gratings, and microstructured fibers. One of the new methods in fiber optics is controlling the propagation of radiation in optical fibers by means of cladding modes.

O V Ivanov Ulyanovsk Branch of the Institute of Radioengineering and Electronics, Russian Academy of Sciences,
ul. Goncharova 48, 432011 Ulyanovsk, Russian Federation
Tel. (7-8422) 442 974
E-mail: olegivvit@yandex.ru
S A Nikitov, Yu V Gulyaev Institute of Radioengineering and Electronics, Russian Academy of Sciences,
ul. Mokhovaya 11, str. 7, 125009 Moscow, Russian Federation
Tel. (7-495) 203 97 88, 203 60 78
E-mail: nikitov@cplire.ru

Received 11 May 2005, revised 19 October 2005
Uspekhi Fizicheskikh Nauk **176** (2) 175 – 202 (2006)
Translated by M V Chekhova; edited by A M Semikhatov

1.1 Core and cladding modes

A usual optical fiber consists of a doped silica core with the diameter ranging from 2 to 8 μm for single-mode fibers, a pure-silica cladding with an external radius equal to several dozen microns, and a polymer coating that protects the cladding from external influence.

Optical fibers are designed for guiding radiation through the core, while the cladding provides total internal reflection of radiation at the boundary with the core, occurring because the refractive index (RI) of the core is few percent higher than that of the cladding. However, the cladding itself is also an optical waveguide and can support optical modes, which, in contrast to the core modes, can be easily scattered or converted even for relatively small deformations and strains of the fiber, and may escape the cladding. Due to its considerable size, the silica cladding of the fiber can support a very large number of modes (for a fiber with the polymer coating removed, it can be of the order of tens of thousands). In practice, one uses modes with small azimuthal numbers and the radial numbers from one to ten.

1.2 Methods of exciting cladding modes

There are several methods of exciting cladding modes. Most often, fiber gratings are used for this purpose. The gratings provide inter-mode coupling, and if the resonance condition is satisfied and the overlap integrals are nonzero, the energy of a core mode can be converted into the energy of a cladding mode. For instance, counter-propagating cladding modes can

be excited by means of fiber Bragg gratings (FBGs) with periods of the order of the radiation wavelength. Cladding modes can also be excited by long-period fiber gratings (LPFGs) with periods from 100 to 1000 μm, which couple the copropagating modes of the core and the cladding.

Bending of the optical fiber can cause the incidence angle for the radiation at the core – cladding boundary to become less than the critical one. The condition for the total internal reflection is then violated and the mode energy leaves the core mode and propagates through the cladding. Radiation can be fed into the core directly, through the butt-end of the optical fiber. It can also be coupled into or out of the cladding by means of tunneling through contact with another fiber or a planar waveguide.

1.3 Special features of cladding mode propagation

There are no principal differences between the cladding modes and the core modes, except that they have different transverse intensity distributions. For a core mode, most of the flux goes through the core and only a small part propagates through the cladding, the field amplitude at the cladding external boundary being vanishingly small. For a cladding mode, the field is distributed over the whole silica cladding and decreases only in the vicinity of its external boundary.

Some part of the cladding mode field penetrates through the external boundary; therefore, cladding modes are quite sensitive to the parameters of the medium surrounding the silica cladding. As a rule, the RI of the polymer coating protecting the cladding is higher than the RI of silica. Therefore, if the polymer coating is not removed, cladding modes are leaky, because there is no total external reflection at the silica – polymer boundary. However, for cladding modes to exist, it is sufficient to provide a small RI difference at the external boundary. For several dozen cladding modes, the incidence angle is rather large, and therefore the usual Fresnel reflection occurs. As a cladding mode propagates through a fiber, it gradually loses energy due to the radiation leakage into the polymer coating, where the radiation is soon absorbed.

The cladding is a multimode optical fiber and, hence, the dispersion properties of its modes are considerably different from the dispersion properties of the core modes. The effective refractive indices (ERIs) of the cladding modes are close to each other but are much smaller than the ERIs of the core. This difference in the dispersion properties is used, for instance, for obtaining double resonances between the core and cladding modes in the spectra.

1.4 Brief summary of the paper

The present paper is devoted to the study of the propagation, excitation, and interaction of cladding modes in optical fibers. In Section 2, we describe the methods for calculating field profiles and propagation constants of cladding modes. The method for obtaining the exact solution in the case of a step-index profile of the fiber and the approximate method valid in the case of an arbitrary profile in the paraxial approximation are reviewed. Dispersion of the cladding modes is described. The properties of leaky and radiation modes are discussed.

In Section 3, we analyze the resonant interaction between core and cladding modes induced by using fiber Bragg gratings. Transmission spectra of FBGs are presented, with multiple loss dips appearing at wavelengths shorter than the Bragg wavelengths. Excitation of azimuthally asymmetric cladding modes with the help of tilted gratings is considered. The methods for suppressing cladding resonances in the transmission spectra of Bragg gratings are described. Experimental spectra of FBGs in microstructured fibers are presented.

In Section 4, the most commonly used method for the excitation of cladding modes is considered, based on using LPFGs. Transmission spectra of LPFGs are calculated. Various methods of fabricating LPFGs are described, including photoinduction and microbending. Special features of the transmission spectra of LPFGs in microstructured fibers are demonstrated. Nonlinear and polarization effects in LPFGs are analyzed. Ways of tuning LPFGs and using them as sensors, gain equalizers in fiber amplifiers, and devices for coupling light into and out of optical fibers are discussed. Cascaded gratings consisting of two LPFGs and phase-shifted gratings are considered.

We note several research centers studying cladding modes and their propagation: the University of Rochester and Corning Incorporated in the USA, the Kwangju Institute of Science and Technology in the Republic of Korea, and the University of Southampton and Aston University in Great Britain. In Russia, such studies are mainly concentrated in the Fiber Optics Science Center of the General Physics Institute of RAS.

Among the numerous publications on the propagation of cladding modes in optical fibers, Russian-language papers on this subject are very few. Therefore, we considered it important to present a paper that would acquaint readers the with the progress in this field.

2. Modes of optical fibers

In this paper, we consider single-mode optical fibers; therefore, we assume that the RI difference for the core and the cladding is small ($\Delta \sim 10^{-2}$) and the core diameter is several microns. In this case, the core is a weakly guiding waveguide and its field almost vanishes at the external boundary of the cladding. Hence, a sufficiently accurate description for a core mode is provided within the approximation of linearly polarized mode. The situation becomes more complicated in the case of cladding modes, whose propagation essentially depends on the boundary between the cladding and the coating. Cladding modes are reflected at this boundary and hence the contrast parameter is considerable. In the case where the cladding is surrounded by air, it is as large as 0.44.

For fibers with step-index profiles, one can obtain exact analytic expressions for mode field distributions and the dispersion relation, whose solution yields the propagation constants for the modes [1, 2].

2.1 Exact solution

To describe the propagation of cladding modes in an optical fiber in the simplest way, we must consider a structure consisting of at least three layers: the core, the cladding, and the surrounding medium. The solution of the three-layer problem was obtained explicitly in Ref. [3] by using the general method developed in Ref. [1] for an arbitrary number of layers. In this section, we briefly review the matrix method of calculating the cladding modes of a multi-layer cylindrical optical fiber with an arbitrary number of layers, similar to the method in Ref. [1].

We consider an optical fiber with a step-index azimuthally symmetric profile of the dielectric permittivity $\varepsilon(r)$. For a

cylindrical fiber, the electric and magnetic fields have the forms

$$\mathbf{E}(r,\varphi,z,t)=\mathbf{E}(r)\exp\left[\mathrm{i}(\beta z-\omega t+v\varphi)\right],$$
$$\mathbf{H}(r,\varphi,z,t)=\mathbf{H}(r)\exp\left[\mathrm{i}(\beta z-\omega t+v\varphi)\right], \quad (1)$$

where β is the propagation constant, ω is the cyclic frequency, and v is the azimuthal number. From the Maxwell equations written in cylindrical coordinates, we can obtain scalar differential equations for the longitudinal components of the electric and magnetic fields. In the general case, the solution of these equations can be written in terms of the Bessel functions,

$$E^{(z)}=\mathrm{i}\,\frac{u^2}{k_0\varepsilon}\left(AJ_v(ur)+BY_v(ur)\right),$$
$$H^{(z)}=-\frac{u^2}{k_0}\left(CJ_v(ur)+DY_v(ur)\right), \quad (2)$$

where $k_0=\omega/c$ is the wave number and $u=\sqrt{k_0^2\varepsilon-\beta^2}$ is the transverse wavevector component, which is real for radially oscillating fields and imaginary for fields exponentially decaying far from the boundary. The tangent and radial field components with respect to the boundaries between the fiber layers can be found from $E^{(z)}$ and $H^{(z)}$. The values of $E^{(r)}$, $H^{(z)}$, and $H^{(\varphi)}$ are real, while $E^{(\varphi)}$, $E^{(z)}$, and $H^{(r)}$ are imaginary. To find the solution in the case of a multilayer cylindrical fiber, we must specify boundary conditions for the tangent field components, as well as the conditions that the field amplitudes are finite at the fiber center and decay at infinity. We let the variables relating to a certain cylindrical layer of the fiber be denoted by the subscript i ($i=1,2,...,a$).

For fields in the central cylinder that are tangent to the boundaries, we can write, in matrix form,

$$\begin{pmatrix}\mathrm{i}k_0E^{(z)}\\-k_0H^{(z)}\\\mathrm{i}E^{(\varphi)}\\H^{(\varphi)}\end{pmatrix}=\begin{pmatrix}-\frac{u_1^2}{\varepsilon_1}J_v(u_1r)&0&0&0\\0&0&u_1^2J_v(u_1r)&0\\\frac{\sigma}{r\varepsilon_1}J_v(u_1r)&0&-u_1J_v'(u_1r)&0\\-u_1J_v'(u_1r)&0&\frac{\sigma}{r}J_v(u_1r)&0\end{pmatrix}\begin{pmatrix}A_1\\0\\C_1\\0\end{pmatrix}$$
$$=M_1\begin{pmatrix}A_1\\0\\C_1\\0\end{pmatrix}, \quad (3)$$

where $\sigma=\beta v/k_0$. In the next cylindrical layers, the tangent fields have the form

$$\left(\mathrm{i}k_0E^{(z)},-k_0H^{(z)},\mathrm{i}E^{(\varphi)},H^{(\varphi)}\right)^{\mathrm{T}}=M_i\left(A_i,B_i,C_i,D_i\right)^{\mathrm{T}}, \quad (4)$$

where

$$M_i=\begin{pmatrix}-\frac{u_i^2}{\varepsilon_i}J_v(u_ir)&-\frac{u_i^2}{\varepsilon_i}Y_v(u_ir)&0&0\\0&0&u_i^2J_v(u_ir)&u_i^2Y_v(u_ir)\\\frac{\sigma}{r\varepsilon_i}J_v(u_ir)&\frac{\sigma}{r\varepsilon_i}Y_v(u_ir)&-u_iJ_v'(u_ir)&-u_iY_v'(u_ir)\\-u_iJ_v'(u_ir)&-u_iY_v'(u_ir)&\frac{\sigma}{r}J_v(u_ir)&\frac{\sigma}{r}Y_v(u_ir)\end{pmatrix}. \quad (5)$$

The condition that the field decays outside the fiber implies that the value of $k_0^2\varepsilon_a-\beta^2$, where ε_a pertains to the surrounding medium, is negative, and the parameters A_a and C_a are equal to zero. For the external layer, we then have

$$\left(\mathrm{i}k_0E^{(z)},-k_0H^{(z)},\mathrm{i}E^{(\varphi)},H^{(\varphi)}\right)^{\mathrm{T}}=M_a\left(0,B_a,0,D_a\right)^{\mathrm{T}}, \quad (6)$$

where

$$M_a=\begin{pmatrix}0&\frac{w_a^2}{\varepsilon_a}K_v(w_ar)&0&0\\0&0&0&-w_a^2K_v(w_ar)\\0&\frac{\sigma}{r\varepsilon_a}K_v(w_ar)&0&-w_aK_v'(w_ar)\\0&-w_aK_v'(w_ar)&0&\frac{\sigma}{r}K_v(w_ar)\end{pmatrix},$$

K_v are the modified Bessel functions, and $w_a=(\beta^2-k_0^2\varepsilon_a)^{1/2}$. The boundary conditions can be expressed in the matrix form as

$$M_1(r_1)(A_1,0,C_1,0)^{\mathrm{T}}=M(0,B_a,0,D_a)^{\mathrm{T}},$$
$$M=M_2(r_1)\,M_2^{-1}(r_2)\,M_3(r_2)\ldots M_{a-1}^{-1}(r_{a-1})\,M_a(r_{a-1}). \quad (7)$$

Using the elements m_{ij} and $m_{ij}^{(1)}$ of the respective matrices M and M_1, we can rewrite relation (7) as

$$N\,(A_1,B_a,C_1,D_a)^{\mathrm{T}}=0,$$
$$N=\begin{pmatrix}-m_{11}^{(1)}&m_{12}&-m_{13}^{(1)}&m_{14}\\-m_{21}^{(1)}&m_{22}&-m_{23}^{(1)}&m_{24}\\-m_{31}^{(1)}&m_{32}&-m_{33}^{(1)}&m_{34}\\-m_{41}^{(1)}&m_{42}&-m_{43}^{(1)}&m_{44}\end{pmatrix}. \quad (8)$$

By setting the determinant of the matrix N equal to zero, we obtain an equation with a single unknown variable β,

$$\det N=0, \quad (9)$$

whose solution is a set of propagation constants for various modes. Substituting the resulting values of β in (8), we can obtain, up to an arbitrary common factor, A_1, B_a, C_1, and D_a, and then the rest of the A_i, B_i, C_i, and D_i, and, finally, the mode fields.

To calculate the core modes, we should replace the oscillating Bessel functions J_v and Y_v in the matrix describing the cladding field by the respective modified functions I_v and K_v, and substitute u_i for w_i. For a cladding of a sufficiently large radius, the core mode amplitude at the external boundary is vanishingly small; therefore, in the calculation of the core modes, the medium surrounding the fiber cladding is usually ignored.

2.2 The weak guidance approximation and the paraxial approximation

In spite of the considerable difference between the RIs of the cladding and the core, a good approximation is often that of weak guidance. The advantage of this approximation is that it can be easily applied to fibers with arbitrary gradient profiles of the RI, for instance, to dispersion-shifted fibers, which have triangular RI profiles. The weak guidance approximation is also relatively simple because it operates with transverse linearly polarized modes and the scalar wave equation.

In the case of cladding modes, it is more correct to use the paraxial approximation, because the RI difference between

the cladding and the coating is not a small value. Because this paper deals with the propagation of low-order core and cladding modes in standard single-mode fibers, the paraxial approximation is applicable here. Within this approximation, it is assumed that the modes propagate almost parallel to the fiber axis and the relative difference between the mode ERI and the cladding RI, $\delta = (n_{\text{eff}} - n_{\text{cl}})/n_{\text{cl}}$, is small, where $n_{\text{eff}} = \beta/k_0$. The relative RI difference between the cladding and the core, $\Delta = (n_{\text{co}} - n_{\text{cl}})/n_{\text{cl}}$, is also assumed to be small, i.e., the core is considered a weakly guiding waveguide. Because the propagation directions of low-order modes almost coincide with the fiber axis, the longitudinal field components of these modes are rather small. Therefore, in the zeroth-order paraxial approximation, the transverse field components can be written as [4]

$$
\begin{aligned}
&\mathrm{HE}_{vm}: E^{(r)} = E_{\lambda m}(r), \quad E^{(\varphi)} = \mathrm{i}\,\mathrm{sign}(v)\, E_{\lambda m}(r)\,,\\
&\quad H^{(r)} = -\mathrm{sign}(v)\,\frac{\mathrm{i}\beta_{\lambda m}}{\omega\mu_0}\,E_{\lambda m}(r)\,,\\
&\quad H^{(\varphi)} = \frac{\beta_{\lambda m}}{\omega\mu_0}\,E_{\lambda m}(r)\,, \quad \lambda = |v| - 1\,;\\
&\mathrm{EH}_{vm}: E^{(r)} = E_{\lambda m}(r)\,, \quad E^{(\varphi)} = -\mathrm{i}\,\mathrm{sign}(v)\, E_{\lambda m}(r)\,,\\
&\quad H^{(r)} = \mathrm{i}\,\mathrm{sign}(v)\,\frac{\beta_{\lambda m}}{\omega\mu_0}\,E_{\lambda m}(r)\,,\\
&\quad H^{(\varphi)} = \frac{\beta_{\lambda m}}{\omega\mu_0}\,E_{\lambda m}(r)\,, \quad \lambda = |v| + 1\,;
\end{aligned}
\tag{10}
$$

$$
\begin{aligned}
&\mathrm{TE}_{0m}: E^{(r)} = 0\,, \quad E^{(\varphi)} = \mathrm{i}\,E_{1m}(r)\,,\\
&\quad H^{(r)} = -\frac{\mathrm{i}\beta_{1m}}{\omega\mu_0}\,E_{1m}(r)\,, \quad H^{(\varphi)} = 0\,;\\
&\mathrm{TM}_{0m}: E^{(r)} = E_{1m}(r)\,, \quad E^{(\varphi)} = 0\,,\\
&\quad H^{(r)} = 0\,, \quad H^{(\varphi)} = \frac{\beta_{1m}}{\omega\mu_0}\,E_{1m}(r)\,,
\end{aligned}
$$

where positive and negative v correspond to right and left circularly polarized modes, respectively. The longitudinal field components for all modes are equal to zero. The function $E_{\lambda m}(r)$ satisfies the equation

$$
E''_{\lambda m} + \frac{1}{r}\,E'_{\lambda m} + \left(k_0^2\varepsilon(r) - \beta_{\lambda m}^2 - \frac{\lambda^2}{r^2}\right)E_{\lambda m} = 0\,, \tag{11}
$$

with the primes denoting derivatives in the radial coordinate.

In the case of a step-index profile of the fiber, the solution of Eqn (11) can be obtained as follows. The general solution is represented in the form

$$
E_{\lambda m} = AJ_\lambda(ur) + BY_\lambda(ur)\,. \tag{12}
$$

The boundary conditions, which ensure the continuity of the field $E_{\lambda m}(r)$ and its first derivative, can be written in the matrix form similarly to (7):

$$
M_1(r_1)(A_1, 0)^{\mathrm{T}} = M(0, B_a)^{\mathrm{T}}\,, \tag{13}
$$

where

$$
M_i = \begin{pmatrix} J_\lambda(u_i r) & Y_\lambda(u_i r) \\ u_i J'_\lambda(u_i r) & u_i Y'_\lambda(u_i r) \end{pmatrix},\ M_a = \begin{pmatrix} 0 & K_\lambda(w_a r) \\ 0 & w_a K'_\lambda(w_a r) \end{pmatrix}, \tag{14}
$$

and M is defined in the same way as in (7). Equation (13) can be written as

$$
N(A_1, B_a)^{\mathrm{T}} = 0\,, \quad N = \begin{pmatrix} -m_{11}^{(1)} & m_{12} \\ -m_{21}^{(1)} & m_{22} \end{pmatrix}. \tag{15}
$$

Setting the determinant of the matrix N equal to zero, we obtain an equation for a single unknown β,

$$
\det N = 0\,, \tag{16}
$$

whose solution is a set of propagation constants for various modes in the paraxial approximation. Substituting the obtained values of β in (15), we can find, up to an arbitrary common factor, the values of A_1 and B_a, and then A_i and B_i for the intermediate layers.

Linearly polarized modes can be obtained as exact superpositions of two, three, or four hybrid modes found in the zeroth-order paraxial approximation (10). In the general case, a linearly polarized mode is the sum of two right circularly polarized modes and two left circularly polarized modes,

$$
\mathrm{LP}_{\lambda,m} = \mathrm{HE}_{\lambda+1,m} + \mathrm{HE}_{-(\lambda+1),m} + \mathrm{EH}_{\lambda-1,m} + \mathrm{EH}_{-(\lambda-1),m}\,. \tag{17}
$$

The modes LP_{0m} and LP_{1m} are special cases:

$$
\begin{aligned}
&\mathrm{LP}_{0,m} = \mathrm{HE}_{1,m} + \mathrm{HE}_{-1,m}\,,\\
&\mathrm{LP}^{(a)}_{1,m} = \mathrm{HE}_{2,m} + \mathrm{HE}_{-2,m} + \mathrm{TE}_{0,m}\,,\\
&\mathrm{LP}^{(b)}_{1,m} = \mathrm{HE}_{2,m} + \mathrm{HE}_{-2,m} + \mathrm{TM}_{0,m}\,.
\end{aligned}
\tag{18}
$$

Usually, the zeroth-order paraxial approximation provides a simple and clear description of mode interaction in optical fibers. But this approximation is not quite valid for some problems where propagation of cladding modes is considered. One such problem is propagation of modes in twisted fibers [4]. The zeroth-order approximation is not valid here primarily because it neglects the longitudinal field components. It can be improved by introducing corrections of higher order in the parameter δ. Equations (10) were obtained by taking only zeroth-order terms in this parameter into account. If terms of the order of $\delta^{1/2}$ are taken into account, nonzero longitudinal components of the field appear, and the modes become not linearly polarized but hybrid.

Using Eqn (10) as the first approximation and substituting it in the Maxwell equations, we find

$$
\begin{aligned}
&\mathrm{HE}_{vm}: E^{(z)} = \frac{\mathrm{i}}{\beta_{\lambda m}}\left(E'_{\lambda m} - \frac{\lambda}{r}\,E_{\lambda m}\right),\\
&\quad H^{(z)} = -\mathrm{i}\,\mathrm{sign}(v)\,\frac{\beta_{\lambda m}}{\omega\mu_0}\,E^{(z)}\,, \quad \lambda = |v| - 1\,,\\
&\mathrm{EH}_{vm}: E^{(z)} = \frac{\mathrm{i}}{\beta_{\lambda m}}\left(E'_{\lambda m} + \frac{\lambda}{r}\,E_{\lambda m}\right),\\
&\quad H^{(z)} = \mathrm{i}\,\mathrm{sign}(v)\,\frac{\beta_{\lambda m}}{\omega\mu_0}\,E^{(z)}\,, \quad \lambda = |v| + 1\,,\\
&\mathrm{TE}_{0m}: E^{(z)} = 0\,, \quad H^{(z)} = \frac{1}{\omega\mu_0}\left(E'_{1m} + \frac{1}{r}\,E_{1m}\right);\\
&\mathrm{TM}_{0m}: E^{(z)} = \frac{\mathrm{i}}{\beta_{1m}}\left(E'_{1m} + \frac{1}{r}\,E_{1m}\right), \quad H^{(z)} = 0
\end{aligned}
\tag{19}
$$

for the longitudinal components. For low-order modes, the relative part of the longitudinal field components is 4 – 10%.

The transverse components include corrections of the order of δ; in contrast to longitudinal components, they do not play a considerable role in the description of any phenomena.

2.3 Field profiles and dispersion of cladding modes

With the help of the method considered in Section 2.1, we have calculated the cladding mode structure for a three-layer optical fiber with the following parameters: $n_{co} = 1.4492$, $n_{cl} = 1.444$, $r_{co} = 4.1$ μm, and $r_{cl} = 62.5$ μm. The wavelength is assumed to be $\lambda = 1.55$ μm. As an example, Fig. 1 shows distribution profiles of the electric field normalized to the energy flux of the corresponding mode. For several cladding modes, namely, HE_{12}, EH_{11}, TM_{01}, and HE_{14}, the radial field components are shown. For all listed modes except TM_{01}, the azimuthal field component practically coincides with the radial one, and the longitudinal field is one order of magnitude smaller than the transverse fields. The azimuthal field for the TM_{01} mode is equal to zero. Even a small deviation of the core RI from the cladding RI has a considerable effect on the mode field distribution; therefore, the approximation where the fiber core is neglected [5] is a crude one. The HE_{1m} modes have a noticeable maximum at the center of the core. For the EH_{1m} modes, on the contrary, the field amplitude is close to zero at the center.

Experimentally measured distributions of the field intensity for two cladding modes, HE_{15} and HE_{16}, are shown in Figs 2a and 2b [6]. The cladding modes were excited by means of an LPFG in a single-mode fiber with the numerical aperture 0.23 and the respective diameters of the core and the cladding 3.5 and 125 μm. One can see that the modes have perfect azimuthal symmetry corresponding to the azimuthal mode number 1 and the number of rings in the cladding is equal to the radial mode number. The bright spot at the center, formed by the core mode, makes it difficult to observe the inner rings of the cladding modes.

For a fixed azimuthal number, Eqn (9) has a set of solutions with two alternating types of modes. For instance, at $v = 0$, odd solutions are TE-modes and even solutions are TM-modes; for $v \geqslant 1$, odd solutions correspond to HE-modes and even solutions to EH-modes. In some papers, including work by T Erdogan, one of the most cited authors [3, 7], cladding modes are numbered without distinguishing between the HE- and EH-modes. In the present paper, we distinguish between these two mode types. The second index

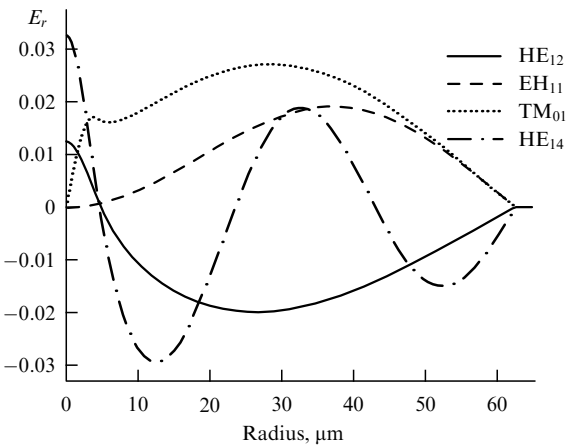

Figure 1. Distribution profiles of the electric field radial component for several cladding modes of an optical fiber.

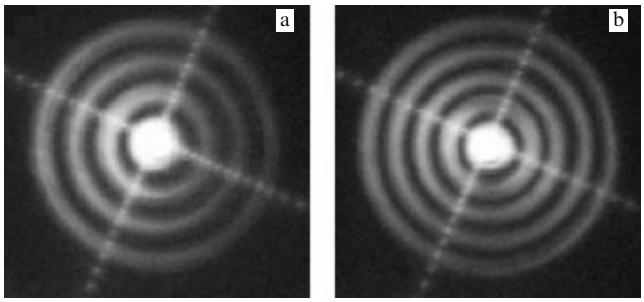

Figure 2. Photographs showing the intensity distributions of HE_{15} (a) and HE_{16} (b) cladding modes [6].

in the notation for cladding modes indicates the radial mode number, which equals the number of intensity maxima in the radial distribution of the field flux. In Refs [3, 7], the core mode is distinguished from the total set of modes, and the cladding modes' radial numbering starts from the first cladding mode and not from the core mode.

The core modes and the cladding modes have different phase propagation velocities. The phase velocity is directly related to the ERI of the mode, which is defined as the ratio of the propagation constant to the wave number in the vacuum, $n_{eff} = \beta/k_0$. The ERI of the core modes are between the RI values of the core and the cladding. The ERI of the cladding modes are below the RI values of the cladding.

Waveguide dispersion manifests itself in the wavelength dependence of the ERI of a mode. This dependence originates from the fact that the field distribution in a fiber depends on the ratio of the fiber size to the wavelength. If variation of λ changes this ratio, then the relative parts of the optical flux propagating to the core, the cladding, and the coating also change. Because the RIs of different layers are different, the ERI of the mode changes as well.

The other type of dispersion that is present in optical fibers is material dispersion. Usually, material dispersion has little effect on the properties of the cladding modes because it almost equally changes the RIs of the core and the cladding. If the RI variation is the same for the core and the cladding, the mode profiles remain almost the same, while the ERI of the core and cladding modes vary by a value equal to the change of the fiber material PI due to the wavelength change. A slight variation of the coating RI has almost no effect on the mode properties because only a small part of the guided field penetrates the coating.

Figure 3 shows the dependences of ERI on the wavelength λ for various mode types of a single-mode optical fiber with the parameters given above. Solid lines correspond to the HE_{1m+1} modes, dashed lines to the EH_{1m} modes, and dotted lines to the TM_{1m} modes. The numbers on the right-hand side of the figure are the radial mode numbers. The highest curve corresponds to the core mode; at large wavelengths, its n_{eff} approaches n_{cl}. This curve has a concave shape, which corresponds to a positive second derivative in the wavelength. The curves below $n_{cl} = 1.444$ correspond to the cladding modes. They also decrease with increasing λ, the tilt being larger for higher-order modes. For low-order modes, the tilt is less than that for the core mode. At some radial number, the tilt of the ERI of one cladding mode becomes equal to the tilt of the core mode curve.

At considerably smaller λ, the fiber becomes multimode i.e., it can guide more than one mode. We see from the figure

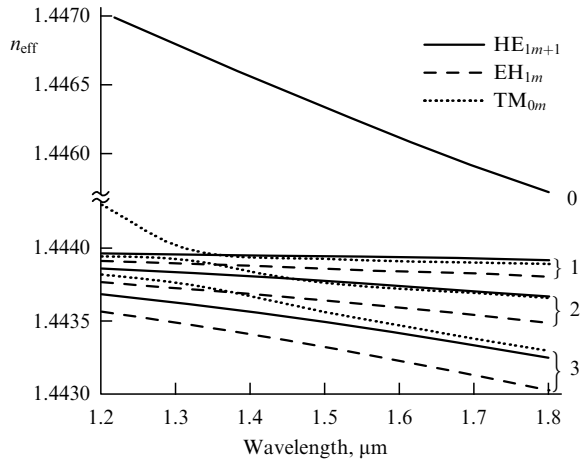

Figure 3. Wavelength dependences of the ERI for the core mode and several cladding modes. The curve numbers correspond to the index m.

that at $\lambda \leqslant 1.3$ μm, the ERI of the cladding TM_{01} mode exceeds n_{cl}, i.e., the cladding mode becomes a core mode.

2.4 Leaky and radiation modes

When the RI of the fiber coating exceeds the RI of the cladding, the condition for the total internal reflection at the outer boundary of the cladding is no longer satisfied, and the parameter w_a becomes imaginary. In this case, the field distribution for $r > r_{\text{cl}}$ is described by nonmodified Bessel functions, which oscillate with the increase in r and do not tend to zero as $r \to \infty$. Such a mode propagates within the whole infinite space and is a radiation mode.

However, even in this case, propagation of light in an optical fiber can be approximately described by the set of modes obtained for a fiber with a coating whose RI is less than the cladding RI. In this case, the modes existing due to the Fresnel reflection at the cladding – coating boundary become decaying, because the energy penetrates the outer space. In other words, such modes are leaking in the course of their propagation. The energy losses for cladding modes propagating along the fiber can also be treated as losses caused by the coupling between these modes and the radiation modes. Propagation of a radiation mode can be described in terms of a complex propagation constant,

$$\beta = \beta_{\text{r}} - \text{i}\beta_{\text{i}}\,, \tag{20}$$

where β_{r} corresponds to the phase velocity of some particular mode and β_{i} corresponds to its attenuation coefficient.

In the description of leaky modes, a common problem is that the fields of such modes are nonzero outside the fiber layers and may increase with the distance from it. This feature makes it difficult to use traditional methods of mode propagation analysis.

If the RI of the coating is larger than the RI of the cladding and the core, which is the case for real optical fibers, the core modes are leaky as well. However, their leakage is much weaker than that of the cladding modes, due to an exponential decay of the core mode field in the cladding.

As mentioned above, the fields of radiation modes do not decay but oscillate with the distance from the cladding; they are described by the functions J_v and Y_v. The coefficients A_a and C_a for guided cladding modes, in contrast to these coefficients for radiation modes, are nonzero in the general case and represent two additional free variables. Therefore, radiation modes have a continuous spectrum, not a discrete one. The additional free parameter specifies the mode polarization. There exist two independent differently polarized modes, and their arbitrary superposition is also a mode of the fiber. Thus, one can arbitrarily choose two linearly independent orthogonal modes.

Field distributions of a radiation mode can be obtained from the relation

$$M_1(r_1)(A_1, 0, C_1, 0)^{\text{T}} = M(A_a, B_a, C_a, D_a)^{\text{T}}\,. \tag{21}$$

By fixing $A_a = 0$ and $C_a = 1$ or $A_a = 1$ and $C_a = 0$, we obtain modes that are similar, respectively, to the ITE and ITM radiation modes of a two-layer fiber with infinite cladding. By fixing $A_a = k_0 n_{\text{co}}^2$ and $C_a = \pm\beta$, we obtain modes close to the hybrid HE and EH, TE and TM fiber modes that would exist in a cladding coated by a material with a smaller RI.

The effect of the RI of the surrounding medium on the properties of leaky modes can be studied with the help of a simplified two-layer model in which the effect of the core is neglected [8]. Under certain assumptions, the real and imaginary parts of the propagation constant for modes with $v = 1$ can be written as

$$\beta_{\text{r}} = k_0 n_{\text{cl}} \left[1 - \frac{1}{2}\left(\frac{(m + 0.25)\pi}{r_{\text{cl}} k_0 n_{\text{cl}}}\right)^2\right],$$

$$\beta_{\text{i}} = 2\pi\, \frac{n_a^2 + n_{\text{cl}}^2}{r_{\text{cl}} k_0 n_{\text{cl}}^3 \sqrt{n_a^2 - n_{\text{cl}}^2}}\,(m + 0.25)\,. \tag{22}$$

However, as shown in Ref. [3], this approximation does not give the correct field profiles in the fiber; hence, it cannot be used for calculating the mode coupling coefficients.

From the expression for the imaginary part of the propagation constant in Eqn (22), we can see that as the RI of the cladding approaches the RI of the coating ($n_a \to n_{\text{cl}}$), special behavior can be observed, namely, there is a dramatic infinite growth of loss. This effect can be used for designing sensors that are highly sensitive to the RI of the surrounding medium. On the other hand, the ERIs of leaky cladding modes depend on the RI of the surrounding medium less than the ERIs of guided modes, because the field of leaky modes, unlike the field of guided modes, is not confined by the boundary between the cladding and the surrounding medium [9].

Similarly to the case of guided modes, radiative cladding modes can be calculated using the weak guidance approximation and the approximation of linearly polarized modes [10]. The radial distribution for the LP_{0m} modes can be represented as

$$E_\xi(r) = \begin{cases} A_\xi\, J_0(u_1 r)\,, & r < r_{\text{co}}\,, \\ B_\xi\, J_0(u_2 r) + C_\xi\, Y_0(u_2 r)\,, & r_{\text{co}} < r < r_{\text{cl}}\,, \\ D_\xi\, J_0(u_3 r) + E_\xi\, Y_0(u_3 r)\,, & r > r_{\text{cl}}\,, \end{cases} \tag{23}$$

where $\xi = w_3$ is the transverse wavevector component selecting a single mode from a continuous spectrum.

Figure 4 shows the results of numerical simulation for the transverse electric field amplitude in an optical fiber with the parameters given in Section 2.3 and the RI of the surrounding medium $n_a = 1.46$. For the two modes shown in the figure, which have $v = 1$ and RIs $n_{\text{eff}} = 1.44390$ and 1.44395, the

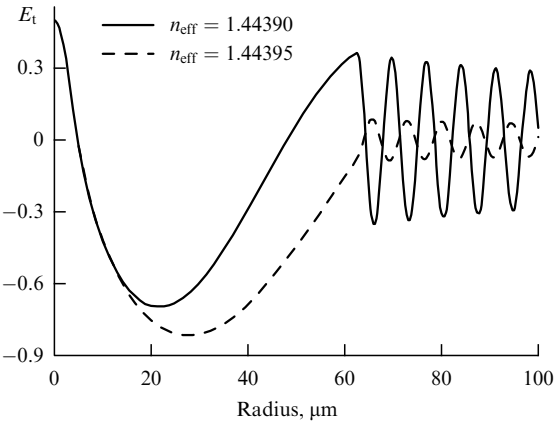

Figure 4. Distribution profile for the electric field transverse component of a radiative mode for two values of its ERI.

field distribution is close to that of the HE_{12} mode. We can see from the figure that even a small difference in the mode ERIs has a significant influence on the field distribution. The oscillation periods in the radial direction are very different in the coating and the cladding, because the wavevector radial component in the cladding, u_2, is much smaller than the corresponding value for the coating, u_3. The amplitude of field oscillations in the coating periodically depends on the ERI because this amplitude is determined by the field at the cladding – coating boundary, which is a periodic function of β. If the ERI decreases, the field distribution becomes more similar to that of the HE_{13} mode, then to that of the HE_{14} mode, etc. The beginning of this process can be seen in the figure as we move from $n_{eff} = 1.44395$ to $n_{eff} = 1.44390$.

Propagation of leaky cladding modes in optical fibers can be analyzed by means of the one-dimensional ray method [11]. Power losses can be calculated in this case from the Fresnel transmission coefficients.

Leaky cladding modes also exist in optical fibers with inner cladding whose RI is less than that of the outer cladding [12]. The cladding modes of microstructured (MS) (photonic-crystal, holey) fibers are leaky [13, 14]. As a rule, such fibers do not have a core with a higher RI and therefore cannot support truly guided modes. Instead, they guide leaky modes, whose energy is gradually lost in the course of propagation by leaking between the holes or through the holes. The study of mode propagation in holey fibers is mostly based on numerical simulation, because the structure of such fibers is rather complex.

There are various numerical methods for calculating the mode structure of holey fibers. One of them is the beam propagation method, which is widely used in studies on complicated waveguide structures and is very convenient for the calculation of leaky modes in MS fibers. We briefly describe the procedure for calculating field profiles and propagation constants of various modes [14]. As the first step, the field at the waveguide input is defined, $E(x, y, 0)$. Then propagation of the field along the waveguide is calculated numerically and $E(x, y, z)$ is found. This calculation does not require knowing the profiles and propagation constants of the modes. We recall that the field in a waveguide can be written as a sum of orthogonal modes,

$$E(x, y, z) = \sum A_j E_j(x, y) \exp(\mathrm{i}\beta_j z), \tag{24}$$

where $E_j(x, y)$ are the profiles of the modes, A_j are their amplitudes, and β_j are their propagation constants.

Knowing the field $E(x, y, z)$ for many values of z, we can use the correlation method to find $E_j(x, y)$, A_j, and β_j for each mode. In this method, first, the correlation function of the initial profile and the profile at a distance z from the input is calculated:

$$P(z) = \int E(x, y, 0)\, E^*(x, y, z)\, \mathrm{d}x\, \mathrm{d}y. \tag{25}$$

Because the modes are orthogonal, $P(z)$ can be simplified:

$$P(z) = \sum |A_j|^2 \exp(\mathrm{i}\beta_j z). \tag{26}$$

The Fourier transform of the correlation function $P(z)$ has sharp peaks at the frequencies corresponding to the propagation constants β_j. The intensities of these peaks give the squared amplitudes of the modes, $|A_j|^2$. The profiles $E_j(x, y)$ can be calculated by taking the values of the Fourier transform $E(x, y, \beta)$ of the function $E(x, y, z)$ at the points β_j:

$$E(x, y, \beta) = \int E(x, y, z)\, \exp(\mathrm{i}\beta z)\, \mathrm{d}z = \sum A_j E_j(x, y)\, \delta(\beta - \beta_j). \tag{27}$$

The scalar beam propagation method was used in Ref. [15] for calculating the mode structure of holey fibers. A separate problem in the study of holey fibers is the calculation of mode losses [13].

3. Fiber Bragg gratings

One of the most common ways to excite cladding modes is based on using fiber gratings, whose technology is rapidly developing. Depending on whether intermode coupling and resonances are introduced between counterpropagating or copropagating modes of an optical fiber, two types of gratings are used: Bragg and long-period, respectively. For the Bragg gratings, the period is of the order of the optical wavelength. For instance, to provide Bragg reflection in a fiber at the wavelength 1.55 μm, the grating period must be equal to 0.54 μm. A fiber Bragg grating is produced by exposing the fiber to ultraviolet (UV) radiation, which induces a periodic modulation of the core RI. To make the UV-radiation intensity periodically vary along the fiber, a two-beam interferometric scheme is applied. Two coherent beams can be produced by means of a beamsplitter, reflections in a prism, or a phase grating. Fiber Bragg gratings are mainly used for coupling two counterpropagating modes of the core. However, in real fibers with a finite cladding diameter, FBGs also excite cladding modes. This effect is sometimes undesirable, and it is then necessary to suppress the coupling between the core and cladding modes.

3.1 Theory

We consider the interaction between the guided modes of the core and the cladding of a standard single-mode fiber in more detail.

In standard fibers, the RI of the core and the cladding differ very little, and therefore, a core mode can be calculated with high accuracy in the LP approximation by assuming that the fiber cladding is infinitely large. The dispersion relation

for an LP core mode has the form

$$V\sqrt{1-b}\,\frac{J_1\left(V\sqrt{1-b}\right)}{J_0\left(V\sqrt{1-b}\right)} = V\sqrt{b}\,\frac{K_1\left(V\sqrt{b}\right)}{K_0\left(V\sqrt{b}\right)}\,, \qquad (28)$$

where $V=(2\pi/\lambda)r_{\rm co}\sqrt{n_{\rm co}^2-n_{\rm cl}^2}$ and $b=(n_{\rm eff}^2-n_{\rm cl}^2)/(n_{\rm co}^2-n_{\rm cl}^2)$ is the normalized ERI. The mode field at the core center is written as

$$E_r^{(\rm co)} = E_{\rm co}J_0\left(V\sqrt{1-b}\,\frac{r}{r_{\rm co}}\right), \quad E_\varphi^{(\rm co)} = {\rm i}E_r^{(\rm co)}\,. \qquad (29)$$

In the cladding, the field of the core mode decays exponentially with the distance from the boundary; therefore, this field is almost equal to zero at the external boundary of the cladding. A cladding mode can be calculated exactly using the method described in Section 2.1.

Because the amplitude of gratings induced by UV radiation is about 10^{-3}, i.e., much less than unity, calculation can be carried out in terms of the coupled mode theory with slowly varying amplitudes. To analyze the mode interaction, we must calculate the coupling coefficients, which can be expressed in terms of mode overlap integrals.

Symmetric FBGs couple modes with the same azimuthal numbers; therefore, the fundamental core mode, which has $v=1$, can be coupled to the HE_{1m} and EH_{1m} modes. The coupling coefficient for two modes is determined by the overlap integral

$$K_{pq} = \frac{\omega\varepsilon_0}{4}\int_\infty \mathbf{E}_p^*(r,\varphi)\,\Delta\varepsilon\mathbf{E}_q(r,\varphi)\,{\rm d}S\,, \qquad (30)$$

where $\Delta\varepsilon$ is the dielectric function variation induced by the UV radiation. In the calculation of coupling coefficients for counterpropagating modes, we can neglect the longitudinal electric field components because they are an order of magnitude less than the transverse components.

When an FBG is induced in an optical fiber, as a rule, only the core RI is changed. Therefore, for photo-induced gratings, $\Delta\varepsilon$ is nonzero only at $r<r_{\rm co}$. In this area, the RI can be written as

$$n(z) = n_{\rm co}\left\{1+\sigma(z)\left[1+M\cos\left(\frac{2\pi z}{\Lambda}\right)\right]\right\}, \qquad (31)$$

where $\sigma(z)$ is a slowly varying envelope, M is the RI modulation amplitude induced in the grating, or the grating visibility, and Λ the grating period. Taking Eqn (31) into account, we can represent the coupling coefficient as $K_{pq}=\kappa_{pq}[1+M\cos(2\pi z/\Lambda)]$, where

$$\kappa_{pq} = \frac{\omega\varepsilon_0}{2}\,n_{\rm co}^2\sigma(z)\int_0^{r_{\rm co}}\mathbf{E}_p^*(r,\varphi)\,\mathbf{E}_q(r,\varphi)\,{\rm d}S\,. \qquad (32)$$

The coupling coefficient κ_{pq} normalized to the RI modulation amplitude in the grating, $\Delta n=n_{\rm co}\sigma(z)$, for the coupling between a core mode and the HE_{1m} and EH_{1m} cladding modes is shown in Fig. 5 [3] as a function of the radial mode number. We see from the figure that the coupling with the EH_{1m} modes having small radial numbers is much weaker than the coupling with the HE_{1m} modes. This is caused by the small amplitudes of the EH_{1m} modes near the core. However, for $m\gtrsim 20$, the HE_{1m} and EH_{1m} modes have comparable coupling coefficients. Slow oscillations in the dependence on the radial mode number are caused by the

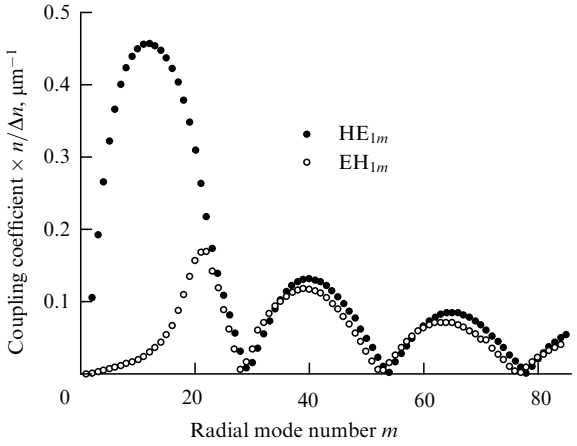

Figure 5. The coupling coefficient for the interaction of HE and EH cladding modes with the core mode as a function of the radial mode number.

fact that when the mode number is increased by unity, the number of oscillations in the field of a cladding mode increases accordingly, and hence the dependence of the mode field on the radial coordinate in the core is shifted towards the fiber center.

In the analysis of the intermode interaction, any coupling between cladding modes can be neglected, including the self-coupling of cladding modes, which leads to corrections in the expressions for the mode propagation constants. This approximation is possible here because only a small part of the cladding mode field is contained in the core, where the grating is induced. Therefore, the overlap integral for two cladding modes is smaller than the overlap integral for a core mode and a cladding mode, which, in turn, is smaller than the overlap integral for two core modes. Using the approximations mentioned above and omitting rapidly oscillating terms, we can obtain a system of coupled-mode equations for the slowly varying amplitudes of the coupled modes [3]:

$$\begin{aligned}
\frac{{\rm d}A^{\rm co}}{{\rm d}z} &= {\rm i}\kappa^{\rm co-co}A^{\rm co} + {\rm i}\,\frac{M}{2}\,\kappa^{\rm co-co}B^{\rm co}\exp(-{\rm i}2\delta^{\rm co-co}z)\\
&\quad + {\rm i}\sum_m\frac{M}{2}\,\kappa_m^{\rm co-cl}B_m^{\rm cl}\exp(-{\rm i}2\delta_m^{\rm co-cl}z)\,,\\
\frac{{\rm d}B^{\rm co}}{{\rm d}z} &= -{\rm i}\kappa^{\rm co-co}B^{\rm co} - {\rm i}\,\frac{M}{2}\,\kappa^{\rm co-co}A^{\rm co}\exp({\rm i}2\delta^{\rm co-co}z)\,,\\
\frac{{\rm d}B_m^{\rm cl}}{{\rm d}z} &= -{\rm i}\,\frac{M}{2}\,\kappa_m^{\rm co-cl}A_m^{\rm co}\exp({\rm i}2\delta_m^{\rm co-cl}z)\,,
\end{aligned} \qquad (33)$$

where A and B denote the respective amplitudes of forward and backward modes and $\delta^{\rm co-co}$ and $\delta_m^{\rm co-cl}$ are mismatch parameters defined as $\delta^{\rm co-co}=(2\beta^{\rm co}-2\pi/\Lambda)/2$ and $\delta_m^{\rm co-cl}=(\beta^{\rm co}+\beta_m^{\rm cl}-2\pi/\Lambda)/2$. Resonant interaction with the cladding modes occurs under the condition

$$\beta^{\rm co}+\Delta\beta^{\rm co}+\beta_m^{\rm cl} = \frac{2\pi}{\Lambda}\,, \qquad (34)$$

with $\Delta\beta^{\rm co}=\kappa^{\rm co-co}$, from which the resonance wavelength can be found. We assume that the resonances are sufficiently narrow and well separated, and hence, for a fixed wavelength, only two waves interact: a core mode and a cladding mode. In this case, a separate resonance with a cladding mode can be selected. If the grating is assumed to be uniform

($\sigma(z) = \text{const}$), then the solution of system (33) yields the reflection and transmission coefficients for this resonance, similar to the reflection and transmission coefficients of a Bragg mirror. (At the center of a resonance, the transmission coefficient is $T = \tanh^2 \kappa L$, where $\kappa = \kappa_m^{\text{co-cl}} M/2$.) The normalized width of the resonance is approximately given by

$$\frac{\Delta\lambda}{\lambda} = \frac{\lambda\kappa}{\pi n_{\text{av}}} \sqrt{1 + \left(\frac{\pi}{\kappa L}\right)^2}, \tag{35}$$

where n_{av} is the average ERI for the two coupled modes.

In the case where the RI of the coating is larger than or close to the RI of the cladding, an FBG cannot excite cladding modes but only radiative ones. For describing coupling with the radiation modes, we replace the sum of the cladding mode fields in the decomposition of the field of an optical fiber by the integral over the continuous spectrum of radiation modes:

$$\mathbf{E} = A^{\text{co}}\mathbf{E}^{\text{co}+} \exp(\mathrm{i}\beta_{\text{co}} z) + B^{\text{co}}\mathbf{E}^{\text{co}-} \exp(-\mathrm{i}\beta_{\text{co}} z) + \int \left[A_\xi \mathbf{E}_{\xi+} \exp(\mathrm{i}\beta_\xi z) + B_\xi \mathbf{E}_{\xi-} \exp(-\mathrm{i}\beta_\xi z)\right] \mathrm{d}\xi\,. \tag{36}$$

Substituting field (36) in the Maxwell equations and neglecting rapidly oscillating terms, we obtain the coupled-mode equations

$$\frac{\mathrm{d}A^{\text{co}}}{\mathrm{d}z} = -\mathrm{i} \int K_\xi^{\text{co-rd}} \exp(\mathrm{i}\varphi_\xi z)\, B_\xi \,\mathrm{d}\xi\,, \tag{37}$$

$$\frac{\mathrm{d}B_\xi}{\mathrm{d}z} = \mathrm{i} K_\xi^{\text{rd-co}} \exp(-\mathrm{i}\varphi_\xi z)\, A^{\text{co}}\,, \tag{38}$$

where $\varphi_\xi = \beta_{\text{co}} + \beta_\xi - 2\pi/\Lambda$. Equations (37) and (38) can be solved by expanding the mode amplitudes A^{co} and B_ξ in the small parameter σM. Keeping the terms up to the second order in this expansion and taking the boundary conditions into account, Koyamada et al. [10] obtained the following expression for the grating transmission coefficient:

$$\frac{A^{\text{co}}}{A_0} = 1 + \int \frac{\alpha_\xi}{\varphi_\xi^2} \left[\mathrm{i}\varphi_\xi L - 1 + \exp(-\mathrm{i}\varphi_\xi L)\right] \mathrm{d}\beta_\xi\,, \tag{39}$$

where $\alpha_\xi = K_\xi^{\text{co-rd}} K_\xi^{\text{rd-co}} (\beta_\xi/\xi)$. Relation (39) is valid under the condition that the energy loss for the core mode is small. If the loss is large, higher-order terms in the expansion should be taken into account. The largest contribution to the integral is given by the domain where $\beta_\xi \approx 2\pi/\Lambda - \beta_{\text{co}}$ and $\varphi_\xi \approx 0$. The behavior of the factor α_ξ determines the FBG transmission at wavelengths corresponding to coupling with radiation modes.

3.2 Transmission spectra

The diagram shown in Fig. 6 illustrates the mode conversion that occurs in an optical fiber in the presence of an RI grating. The whole range where modes exist is divided into three areas: area I contains radiation modes, area II, cladding modes, and area III, core modes. The areas are separated by dashed lines $\beta = n_{\text{co}} k_0$, $\beta = n_{\text{cl}} k_0$, and $\beta = n_a k_0$. Long arrows show intermode coupling caused by fiber Bragg gratings. The length of an arrow is inversely proportional to the grating period, $k_{\text{g}} = 2\pi/\Lambda$. For a small wavenumber (large wavelength), the core mode is coupled to a similar mode propagating in the opposite direction and having negative propagation constants. At somewhat larger k_0 (smaller wavelengths), a core mode becomes coupled to one of the counterpropagating cladding modes; at still larger k_0, the grating converts a core mode into radiation modes.

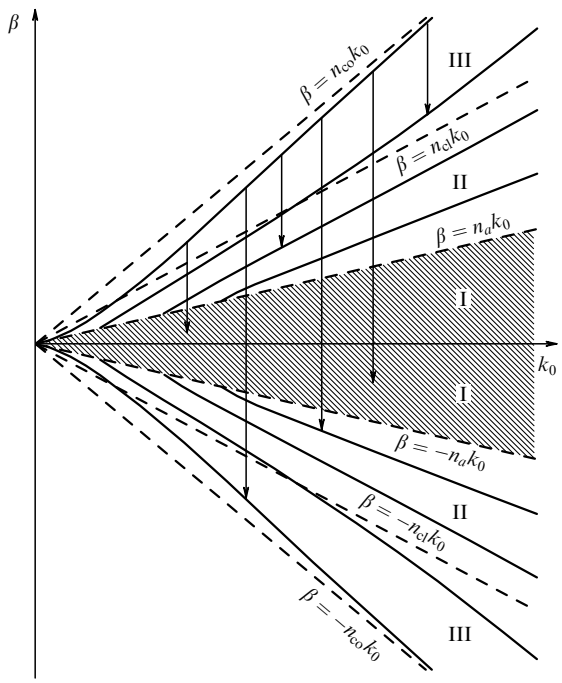

Figure 6. Diagram illustrating mode coupling in an FBG and an LPFG. Solid lines correspond to the propagation constants of the core modes (area I), cladding modes (area II), and radiation modes (area III) as functions of the wavenumber. Dashed lines separating the areas are given by the relations $\beta = n_a k_0$, $\beta = n_{\text{cl}} k_0$, and $\beta = n_{\text{co}} k_0$. Arrows show transitions excited by the Bragg gratings (long arrows) and long-period gratings (short arrows).

Figure 7 shows the transmission spectra calculated for an FBG with the period $\Lambda = 530$ nm, length 0.5 cm, and RI modulation amplitude 5×10^{-4} [10]. Calculations were carried out for the following cases: the RI of the cladding is larger than the RI of the coating (Fig. 7a); the RI of the cladding is equal to the RI of the coating, i.e., cladding modes do not exist (Fig. 7b); the RI of the cladding is smaller than the RI of the coating, i.e., cladding modes are leaky (Fig. 7c). In all three cases, the spectra contain a Bragg reflection peak, its shape and position being practically independent of the RI of the coating. In the short-wavelength part of the spectra (Figs 7a, c), a series of peaks is observed, corresponding to resonances with the HE_{1m} cladding modes. In Fig. 7b, the resonances are absent; instead, there is a continuous absorption spectrum caused by the coupling between the core mode and radiation modes. When the RI of the cladding exceeds the RI of the coating, the energy is most efficiently coupled into cladding modes with $m \approx 11$, because these modes have the largest coupling coefficient with the core modes (see Fig. 5). In Fig. 7a, cladding resonances at $\lambda > 1546$ nm are considerably narrower than the resonances at $\lambda < 1546$ nm. This is because the resonances at wavelengths above 1546 nm are formed by guided cladding modes, while the resonances at wavelengths below that are created by leaky cladding modes. The resonances of leaky cladding modes have smaller amplitudes and are more 'smeared' than the resonances of guided modes. That the cladding supports only a few (16) modes is because of the small difference between the refractive

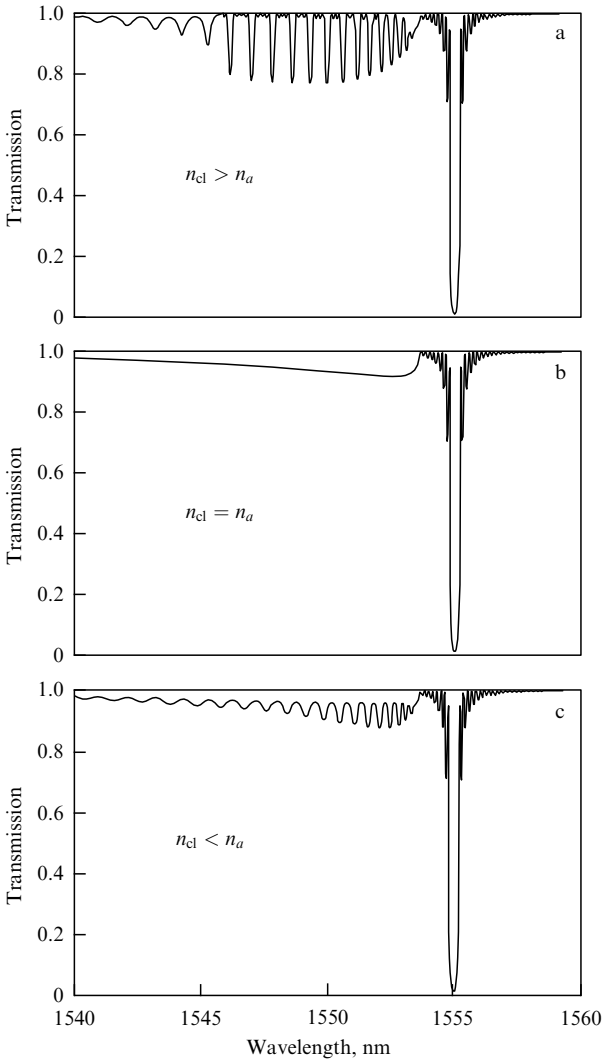

Figure 7. Transmission spectra of an FBG calculated in the cases where the RI of the cladding exceeds the RI of the coating (a), equals it (b), and is smaller (c) [10].

indices of the coating and the cladding assumed in the calculation. In fibers surrounded by air, with more than a hundred modes having $v = 1$, only resonances of guided modes are observed. Experimental spectra measured for fibers of various types are qualitatively the same as the spectra shown in Fig. 7.

As we have already mentioned, the character of the spectrum is determined by the behavior of the factor α_ξ. If the RI of the coating equals the RI of the cladding, this factor has a monotonic dependence on the wavelength (similar to the dependence in Fig. 7b) in the range of cladding-mode resonances. If the RI of the coating exceeds the RI of the cladding, α_ξ has an oscillating dependence (similar to the dependence in Fig. 7c).

3.3 Tilted gratings

In the usual, nontilted gratings, coupling is only possible between modes with equal azimuthal numbers. Therefore, the fundamental core mode HE_{11} can exchange energy only with modes for which $v = 1$, i.e., with the HE_{1m} and EH_{1m} modes. In tilted gratings, mode coupling is more complicated, because in general, coupling can exist between modes with arbitrary azimuthal numbers [16]. A grating can be tilted in two ways with respect to the polarization of the core mode direction: the grating vector can be either in the polarization plane (p-grating) or orthogonal to it (s-grating). The coordinate dependence of the RI variation in the core can be written as

$$\Delta n(x, y, z, \theta) = n_{co}\sigma(z')\left[1 + M\cos\left(\frac{2\pi}{\Lambda}z'\right)\right], \qquad (40)$$

where

$$z' = \begin{cases} z\cos\theta - x\sin\theta, & \text{p–grating,} \\ z\cos\theta - y\sin\theta, & \text{s–grating,} \end{cases}$$

θ is the tilt angle of the grating, and $\sigma(z')$ is the grating envelope, which describes the slow variation of the grating amplitude along the coordinate z'. Interaction of the modes in tilted gratings can be described similarly to the case of non-tilted gratings using the coupled mode theory and calculating the coupling coefficients in terms of the overlap integrals. The coupling coefficients depend on the polarization directions of the modes. Calculations show that the coupling coefficients for modes with orthogonal polarizations are small. Similarly, the coupling coefficient for two cladding modes is small compared with the coupling coefficient for a core mode and a cladding mode, as is the case for nontilted gratings.

The coupling coefficients for the interaction between core and cladding modes in tilted gratings depend on the radial mode number in the same way as the coupling coefficients in nontilted gratings. However, there are still some differences: as a rule, the EH_{2m} and EH_{3m} cladding modes have higher coupling coefficients than the HE_{2m} and HE_{3m} modes; the coupling coefficient decreases with the increase in the azimuthal mode number; the strongest coupling occurs at higher radial numbers than in the case of nontilted gratings. The coupling coefficients have periodic dependences on the grating tilt angle. At the same time, the oscillation amplitude decreases with the increase in the angle. For $v = 1$, the maximum occurs at $\theta = 0$. For $v = 2$, the coupling coefficient is maximal at $\theta = 5°$, and for $v = 3$, at $\theta = 7.5°$; therefore, if a high coefficient of reflection into cladding modes is to be obtained, the tilt angle of the FBG with respect to the fiber axis should not exceed several degrees ($5-10°$) [16].

If tilted gratings in optical fibers are used at wavelengths smaller than the cutoff wavelength, the basic core mode LP_{01} can exchange energy not only with cladding modes but also, and primarily, with higher-order core modes, for instance, with the asymmetric LP_{11} mode [17].

In the measured transmission spectra of tilted FBGs, similarly to the case of nontilted gratings, there are multiple absorption peaks at wavelengths shorter than the Bragg wavelength. These peaks are caused by resonances with the cladding modes. The difference from the case of nontilted gratings is that for a tilted grating, the spectrum is a sequence of alternating resonances with various mode types, which have different azimuthal mode numbers. The largest peaks are the those related to the LP_{0m} and LP_{1m} modes [18, 19]. The spectrum also contains a broad loss band caused by the coupling with radiation modes and overlapping with the resonance peaks of cladding modes. Positions of the resonance peaks and of the band of losses into radiation modes depend on the RI of the surrounding medium; this fact made it possible to propose FBG-based sensors for measuring

RI [19]. If the fiber with an FBG in the core is bent, the angle between the beam and the grating varies, which leads to a change in the coupling coefficient between the forward core mode and the backward cladding mode. As a result, the transmission coefficients at the resonance frequencies of cladding modes also change. Thus, by measuring the transmission coefficient, one can determine the fiber curvature, and a bending sensor can be built based on this principle [20]. Finally, tilted FBGs can be used for constructing a low-loss narrow-band filter [21].

3.4 Suppression of cladding resonances

In Section 3.3, we described possible applications of resonant reflection from an FBG into cladding modes. However, this phenomenon is quite often undesirable, and it is necessary to suppress reflections into cladding modes and eliminate the corresponding losses. In particular, this is the case if only a narrow Bragg band providing reflection into the basic core mode is required. Loss peaks in the short-wavelength part of the spectrum can be extremely harmful, especially in systems with wavelength division multiplexing (WDM). For this reason, active studies on the suppression of cladding resonances are being carried out [22 – 26].

The basic way to suppress cladding resonances is to reduce the coupling coefficients for the interaction between core and cladding modes. This can be achieved by controlling the three parameters determining the coupling coefficients.

First, by choosing the RI profile of an optical fiber, one can vary the field profiles for both core and cladding modes. In particular, it is possible to choose the RF profile that minimizes the mode overlap integrals. As a rule, the coupling coefficients for low-order cladding modes can be suppressed in optical fibers whose cladding contains a ring of reduced RI around the core (depressed cladding) [22]. Such a ring efficiently decreases the field amplitudes of the cladding modes in the core and hence reduces the overlap integrals with the core mode. However, for a fiber with depressed cladding, additional loss peaks are observed in the interval between the Bragg resonance and the cladding resonances. These peaks are caused by the existence of leaky modes in the part of the cladding where the RI is reduced. The amplitudes of these peaks increase considerably when the grating is tilted, even slightly, with respect to the fiber axis. Therefore, accurate positioning of the fiber during the grating writing becomes critical [23].

Second, the mode overlap integrals can be reduced by varying the photosensitivity profile of the fiber [24]. In an ideal case, the cladding should have the same photosensitivity as the core. Then the overlap integral is zero due to the orthogonality of the modes. In practice, it is sufficient to extend the photosensitivity profile by several microns and reach the area where the exponentially decaying amplitude of the core mode approaches zero. As a result, the product of three functions, the photosensitivity and the mode fields of the core and the cladding, is then also close to zero. The photosensitivity profile can be expanded by doping the cladding with germanium and other dopants necessary for compensating the change in the RI. A drawback of this method is the reduction of the grating strength caused by the absorption of UV radiation outside the core, where the core mode has a small amplitude. The most efficient way is to vary both the RI profile and the photosensitivity profile [27]. In order to considerably suppress the cladding resonances, accurate measurement and control of the fiber photosensitivity profile is required. This allows obtaining the values of losses into cladding modes less than 0.1 dB when writing FBGs with strengths up to 30 dB [24].

It is also possible to create gratings with nonstandard distributions of the induced RI over the fiber cross section. Parker and de Sterke [25] suggested a new method of FBG writing in standard fibers, in which the fiber rotates around its axis during the tilted grating writing. Theoretical calculation has shown that cladding modes in such gratings have considerably weaker resonances. However, so far this statement has no experimental evidence.

Third, the influence of cladding resonances in FBGs can be eliminated by increasing the numerical aperture of the fiber, which leads to an increase (up to 10 nm) in the wavelength interval between the Bragg resonance and the multiple resonances of cladding modes. This expands the wavelength range of the Bragg gratings used in WDM systems. An important part of the problem is splicing the special fiber designed for the FBG writing and the standard fiber, because splicing fibers with different RI profiles can introduce additional losses. By optimizing the parameters of the fibers, losses caused by splicing with the standard SMF-28 fiber have been reduced to 0.04 dB.

If the fiber grating writing is not ideal, the methods developed for the ideal case may not be optimal. Indeed, in the case where the normal to the grating forms a small angle with the fiber axis, reflection into cladding modes can grow considerably. To reduce the sensitivity of an FBG to small tilt angles, it was suggested [26] to make the diameter of the cladding area with a reduced RI smaller than its standard value. Such fibers are also less sensitive to a possible azimuthal asymmetry of the induced grating. For large tilt angles ($> 1.3^\circ$), it is reasonable to use fibers with matched cladding.

Finally, the suppression of cladding resonances can be achieved by producing obstacles for the propagation of cladding modes along the fiber. For this, the cladding is covered by an absorbing material or a transparent polymer whose RI coincides with that of the cladding. Attenuation of the cladding modes smears and weakens the corresponding resonances.

3.5 Bragg gratings in microstructured fibers

Many applications of FBGs are based on complex gratings with various profiles, which are written in the usual germano – silicate fibers. The new generation of fiber optical systems requires optical components with greater functionality; therefore, the attention of researchers is focused on the creation of usual gratings in modified waveguide structures with more complex configurations [15, 28, 29]. Modified optical fibers can be divided into two groups, according to the methods of their fabrication: (1) those obtained by processing standard fibers and (2) those with the structure modified in the course of fabrication. In this section, we consider fibers of the second group, namely, microstructured (MS) fibers, which are being intensively studied at present [30].

Microstructured fibers are produced from structured preforms and contain air holes along the whole fiber. Interest in such structures was caused, in particular, by the fact that light can be guided not by the total internal reflection but by the Bragg reflection from the periodic array of holes, as well as by the possibility of generating a supercontinuum [31]. MS fibers provide additional possibilities in the design of devices based on cladding modes, because the sizes of the air gaps and their distribution in the cladding can be controlled. More-

over, air gaps can be filled by various active media, which can be used to control the parameters of gratings induced in such a fiber.

Microstructured fibers can be divided into two classes: photonic-crystal (PC) fibers, in which the holes form a two-dimensional periodic superlattice, and simple holey fibers where holes do not form any periodic structure. In addition, two different mechanisms of wave guiding are possible in MS fibers. In the first case, the wave undergoes Bragg reflection from the periodic structure where it cannot propagate due to the existence of a band gap. This mechanism is only possible in PC fibers. In the other case, total internal reflection occurs at the core–cladding boundary. The condition for total internal reflection is provided by making the RI of the silica core (which may be doped) higher than the average RI of the holey cladding.

The application of MS fibers in communication lines is limited by losses, which are typically larger in such fibers than in standard ones. On the other hand, if MS fibers are used for grating writing, the losses become completely unessential because the lengths of the gratings do not exceed several centimeters.

In some applications, the holes of MS fibers are designed not for guiding core modes but for the control of the cladding modes. In such fibers, a core mode is guided by the doped silica core, as in the case of standard fibers [29]. Doping allows writing photo-induced FBGs and LPFGs in such fibers.

An investigation of the spectra of MS fibers can be used for characterizing both core modes and cladding modes. In particular, transmission spectra of FBGs written in MS fibers manifest resonances related to the cladding modes. These resonances provide information on the mode structure of the fibers, propagation constants, and field profiles for the modes. The obtained characteristics can be used for the design of new optical components based on MS fibers.

The insets in Fig. 8 show four types of MS fibers where gratings were written: a PC fiber (Fig. 8a), a fiber with a 'grapefruit' structure (Fig. 8b), a fiber with inner air cladding (Fig. 8c), and a fiber with a high RI contrast ('high-delta' fiber, Fig. 8d). The cladding of the PC fiber is filled by periodic holes. In the case shown here, light was confined in the fiber not because of the Bragg reflection but due to the existence of the core having no air hole. The properties of an MS fiber are very similar to the properties of the usual fiber with the radius equal to the inner radius of the MS fiber silica cladding. When the inner radius of the cladding becomes close to the core radius, the result is a fiber with a large RI contrast, whose modes are strongly squeezed by the air gaps. Such modes manifest considerable anomalous dispersion in the visible wavelength range.

In fibers of all these types, FBGs were written using phase masks and pulsed UV laser radiation with the wavelength 242 nm [14]. The transmission spectra of the gratings were obtained by measuring the power of laser light transmitted through the fiber, the wavelength of the radiation being scanned within a certain range. At the wavelengths where loss peaks were observed, the profiles of reflected cladding modes were registered by means of a microscope.

A special PC fiber was designed, with the core doped by a small amount of germanium, such that the doping did not introduce noticeable perturbation of the guided modes but was still sufficient for writing a grating. A typical core radius was of the order of 1 μm and the contrast was $\Delta = 5 \times 10^{-3}$. The core of the high-delta fiber had the same parameters. The

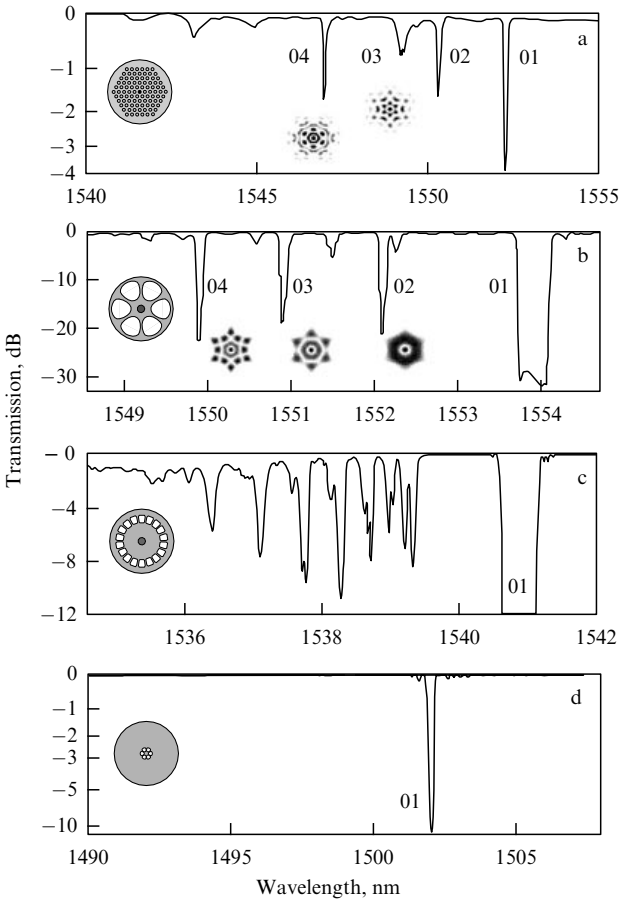

Figure 8. Transmission spectra of FBGs in MS fibers of various types: a PC-fiber (a) a fiber with a 'grapefruit' structure (b), a fiber with inner air cladding (c), and a fiber with a high RI contrast (d) [14]. The insets show the cross sections of the fibers and the profiles of cladding modes corresponding to some resonances.

distance between the holes in the hexagonal lattice was about 10 μm; hence, the modes were confined in the core due to the total internal reflection rather than the Bragg reflection. In fibers with a 'grapefruit' structure and inner air cladding, the core radius was ~ 4 μm and the contrast was $\Delta = 3.5 \times 10^{-3}$.

Figure 8 shows the transmission spectra of gratings written in fibers of the four types described above: a PC fiber (Fig. 8a), a fiber with a 'grapefruit' structure (Fig. 8b), a fiber with inner air cladding (Fig. 8c), and a fiber with a high RI contrast (Fig. 8d). The resonance denoted by '01' in Fig. 8 corresponds to reflection into the core mode. Further resonances, at shorter wavelengths, correspond to leaky cladding modes, which quickly become scattered in the course of their propagation along the fiber. In contrast to the case of usual fibers, the intensity of reflections into cladding modes in PC fibers is comparable to the intensity of reflection into the core mode. This is because several low-order cladding modes propagate close to the fiber core and have large overlap integrals with the core mode. The distance between the cladding-mode resonances is larger in PC fibers than in usual fibers, which is also due to a smaller mode radius. Near the peaks in the spectrum, field profiles for the corresponding excited cladding modes are also shown in the figure.

In the 'grapefruit' fiber, the distance between the cladding resonances is also larger than in standard fibers. The strongest

resonances correspond to the modes whose field profiles are mostly contained in the inner area between six holes. A small part of the light escapes from the fiber through thin silica walls.

The properties of the fiber with inner air cladding are very similar to those of the usual fiber with the outer diameter equal to the inner cladding diameter of the fiber shown in Fig. 8c. The spectrum in Fig. 8c therefore resembles the transmission spectrum of a grating in a standard fiber. The mode profiles of such a fiber have almost circular symmetry; they also have been observed in experiment [14].

The spectrum of the high-delta fiber contains no cladding-mode resonances. This is because the radius of the inner cladding is very small and the RI of the first cladding mode differs significantly from the RI of the core. As a result, this resonance is very far from the Bragg peak. Strictly speaking, in such a fiber, the core mode is already a cladding mode, because its RI is about 1.40, which is less than the cladding RI.

The structure of MS fibers allows them to be filled with various gases or liquids. Westbrook et al. [32] filled the holes with a UV-curable polymer and then exposed it to UV radiation. The refractive index of a polymer depends on the temperature much more strongly than that of fused silica; therefore, the cladding-mode resonances excited by means of an FBG in such a structure are more sensitive to temperature changes than the resonances in usual fibers. This fact has been confirmed experimentally. At room temperature, the RI of the polymer is higher than the RI of silica, but it reduces due to the increase in temperature and may become smaller than the RI of silica in the case of strong heating. Because of this, a temperature variation can lead to a change in the regime of the waveguide propagation of a cladding mode.

Thus, microstructuring optical fibers enables one to control the characteristics of cladding modes in new ways, which are impossible for usual fibers.

4. Long-period fiber gratings

A long-period fiber grating is a fiber structure with the properties periodically varying along the fiber, such that the conditions for the interaction of several copropagating modes are satisfied. The period of such a structure is of the order of a fraction of a millimeter. In contrast to the Bragg gratings, LPFGs couple copropagating modes with close propagation constants; therefore, the period of such a grating can considerably exceed the wavelength of radiation propagating in the fiber. Because the period of an LPFG is much larger than the wavelength, LPFGs are relatively simple to manufacture. Since LPFGs couple copropagating modes, their resonances can only be observed in transmission spectra. The transmission spectrum has dips at the wavelengths corresponding to resonances with various cladding modes (in a single-mode fiber) [33].

Depending on the symmetry of the perturbation that is used to write the LPFG, modes of different symmetries may be coupled. For instance, cylindrically symmetric gratings couple symmetric LP_{0m} modes of the fiber. Microbend gratings, which are antisymmetric with respect to the fiber axis, create a resonance between the core mode and the asymmetric LP_{1m} modes of the core and the cladding.

Various gratings with complex structures have been designed: gratings combining several LPFGs, LPFGs with superstructures, chirped gratings, and gratings with apodization. Various LPFG-based devices have been developed: filters, sensors, fiber dispersion compensators, etc.

4.1 Theory

There are two basic methods of calculating the LPFG transmission spectra. The first is based on the standard coupled-mode theory, which involves the approximations of phase synchronism and weak perturbation, i.e., the assumption that the perturbation introduced into the fiber due to the grating formation has little effect on the fiber mode structure [3, 34]. In the analysis of gratings where the RI profile is not sinusoidal but rectangular, only the zeroth-order and the first-order harmonics are taken into account; contributions of higher-order Fourier harmonics of the grating are neglected.

The second method, known as the transfer-matrix method, is based on dividing the fiber into uniform parts whose cross sections are constant along the fiber [35]. For each part, one calculates the mode structure and the transfer matrix that relates the electromagnetic fields at the input and the output. By multiplying the matrices of different parts, one obtains the matrix describing the whole grating. The transfer-matrix method provides the exact solution to the problem, but it can only be obtained numerically. Used together with the reflection-free approximation and the approximation of weak perturbation of the mode structure [36], this method yields results that are only 2% different from the results of the coupled-mode theory.

There also exists an intermediate method, in which the transfer matrix of a single uniform part of the fiber is found from the coupled-mode theory and then the total transfer matrix is found as a product of matrices for separate layers [37]. This way, the phase matching approximation is not used and all Fourier harmonics of the grating are taken into account. Comparison shows that the transmission spectrum obtained by means of this method differs from the one calculated through the coupled-mode theory by not more than 2.5%.

Propagation and conversion of cladding modes in LPFGs can be studied by numerical methods. For instance, Murtaza et al. [38] used the beam propagation method and the finite-difference method to calculate the transmission spectrum of an LPFG with microbends. The results agree well with the experimental data.

We consider the application of the coupled mode method to an LPFG in more detail. Similarly to the case of an FBG, we consider a photo-induced grating and assume that the RI is varied only in the core of the fiber and is described by Eqn (31). The expression for the mode coupling coefficient in an LPFG has the same form as in the case of an FBG [see Eqn (30)]. Due to the radially symmetric perturbation, the core mode is coupled to the HE_{1m} and EH_{1m} modes of the cladding. For the same reasons as in the case of FBGs, we neglect the interaction between the cladding modes. We take only the mode self-coupling into account, which can shift resonances in the LPFG transmission spectra. Then, neglecting rapidly oscillating terms, we obtain the coupled-mode equations [3]

$$\frac{\mathrm{d}A^{\mathrm{co}}}{\mathrm{d}z} = \mathrm{i}\kappa^{\mathrm{co-co}}A^{\mathrm{co}} + \mathrm{i}\sum_n \frac{M}{2}\,\kappa_n^{\mathrm{co-cl}}A_n^{\mathrm{cl}}\exp(-\mathrm{i}2\delta_n^{\mathrm{co-cl}}z)\,,$$
$$\frac{\mathrm{d}A_m^{\mathrm{cl}}}{\mathrm{d}z} = \mathrm{i}\kappa_m^{\mathrm{cl-cl}}A_m^{\mathrm{cl}} + \mathrm{i}\,\frac{M}{2}\,\kappa_m^{\mathrm{cl-co}}A^{\mathrm{co}}\exp(\mathrm{i}2\delta_m^{\mathrm{co-cl}}z)\,, \tag{41}$$

where $\delta_m^{\text{co-cl}} = (\beta^{\text{co}} - \beta_m^{\text{cl}} - 2\pi/\Lambda)/2$. The resonance condition is given by

$$\beta^{\text{co}} + \Delta\beta^{\text{co}} - \beta_m^{\text{cl}} - \Delta\beta_m^{\text{cl}} = \frac{2\pi}{\Lambda}\,, \tag{42}$$

where $\Delta\beta^{\text{co}} = \kappa^{\text{co-co}}$ and $\Delta\beta_m^{\text{cl}} = \kappa_m^{\text{cl-cl}}$ are corrections to the propagation constants of the core and the cladding modes, which appear because of the mode self-coupling at the zeroth-order Fourier component of the grating RI.

As a rule, cladding mode resonances are rather far from each other in the spectrum. Therefore, in the coupled-mode equations for a certain wavelength, it is sufficient to take only a single cladding mode into account.

For a grating that couples two fiber modes and has a uniform distribution of the induced RI ($\sigma(z) = \text{const}$), the analytic solution of system (41) can be easily obtained. We assume that the fiber modes were calculated with the constant component of σ taken into account, i.e., with the RI of the core assumed to be $n_{\text{co}}(1+\sigma)$. In this case, $\Delta\beta^{\text{co}}$ and $\Delta\beta^{\text{cl}}$ are equal to zero, and the solution of (41) is written as

$$\begin{pmatrix} A^{\text{co}}(L) \\ A_m^{\text{cl}}(L) \end{pmatrix} = \begin{pmatrix} \exp(-\mathrm{i}\delta z) & 0 \\ 0 & \exp(\mathrm{i}\delta z) \end{pmatrix} \times \begin{pmatrix} \cos\eta L + \mathrm{i}\,\dfrac{\delta}{\eta}\sin\eta L & \mathrm{i}\,\dfrac{\kappa}{\eta}\sin\eta L \\ \mathrm{i}\,\dfrac{\kappa^*}{\eta}\sin\eta L & \cos\eta L - \mathrm{i}\,\dfrac{\delta}{\eta}\sin\eta L \end{pmatrix} \times \begin{pmatrix} A^{\text{co}}(0) \\ A_m^{\text{cl}}(0) \end{pmatrix}, \tag{43}$$

where $\eta = \sqrt{\delta^2 + |\kappa|^2}$ and $\kappa = \kappa_n^{\text{co-cl}} M/2$; for brevity, the subscripts of the mismatch parameter are omitted here.

The usual photo-induced gratings couple the core mode with the azimuthally symmetric cladding modes and the HE_{1m} and EH_{1m} modes. Exposure to the UV radiation changes only the RI of the core. In this case, the coupling coefficient for the core mode and hybrid modes depends on the radial mode number as shown in Fig. 5.

In asymmetric gratings, depending on the grating type, the core mode HE_{11} can be coupled to the modes of various polarizations having arbitrary azimuthal and radial numbers. In gratings with microbends, the induced grating has an antisymmetric structure over the fiber cross section, $\Delta\varepsilon(x,y,z) = (x/r_{\text{cl}})\,\Delta\varepsilon_0\cos(2\pi z/\Lambda)$, where $\Delta\varepsilon_0$ is the grating amplitude at the external boundary of the cladding. The only nonzero overlap integrals for the core modes are the ones with the TM_{0m} (TE_{0m}) and HE_{2m} modes. Because these modes are almost degenerate in the paraxial approximation and correspond to the LP_{1m} mode, their resonances overlap with each other and become indistinguishable in the LPFG spectra for fibers of standard radii and modes with small radial numbers.

4.2 Transmission spectra

Resonance coupling between the core mode and other modes of an optical fiber is illustrated in Fig. 6, where short arrows corresponding to LPFGs have the length $k_{\text{g}} = 2\pi/\Lambda$. At large wavelengths (small k_0), a core mode is coupled to radiation modes, at medium wavelengths (medium k_0), to cladding modes, and at small wavelengths (large k_0), to core modes. The order of the modes in the resonance spectrum of an LPFG is reversed compared to the case of an FBG.

We assume that the mode structure of a fiber is calculated with only the constant component of the RI induced by the UV radiation (the zeroth-order Fourier harmonic of the RI) taken into account. The corrections $\Delta\beta^{\text{co}}$ and $\Delta\beta^{\text{cl}}$ to the propagation constants can then be set equal to zero. In this case, the resonance wavelengths are found from the relation

$$\lambda = \left(n_{\text{eff}}^{\text{co}} - n_{\text{eff},\,m}^{\text{cl}}\right)\Lambda\,. \tag{44}$$

It is convenient to find the resonance wavelengths graphically, by plotting the dependence $\Lambda(\lambda)$. The horizontal line corresponding to a certain grating period intersects the resonance curves of the modes at wavelengths where cladding resonances are to be observed (Fig. 9).

The entire spectrum of an LPFG consists of several dips, each one corresponding to a resonance with a certain cladding mode. An example of such a spectrum is shown in Fig. 10 [34]. One can see that the depth of the dips increases as the wavelength grows, which is because higher-order cladding modes have larger coupling coefficients.

The dependences of the grating period on the resonance wavelength $\Lambda(\lambda)$ have smaller tilt for higher-order modes; for some mode number, the dependences become nonmonotonic functions of the wavelength in the range under study. Such a curve can intersect the same horizontal line twice. This is the case for curve *10* in Fig. 9. The transmission spectrum of such a grating has two loss peaks, corresponding to resonances with the same cladding mode [39–41]. Even slight variations in the mode coupling conditions lead to a change in the distance between the two loss peaks.

Gratings with a period close to the peak of the resonance curve $\Lambda(\lambda)$ were used in Ref. [40] to achieve mode coupling in the broadest possible wavelength range. Mode conversion with an efficiency above 99% has been obtained within the range 1525–1588 nm. A special case occurs if the grating period coincides with the peak of a nonmonotonic curve (as for curve *10* in Fig. 10 at the wavelength 1600 nm) [42]. Variation of the coupling conditions at this point would result not in a shift of the resonance wavelength but in a change in the value of the loss.

For even larger mode numbers, the tilt of the curves changes sign. Because of this, the increase in the average RI of the core in the course of the grating writing leads to a shift

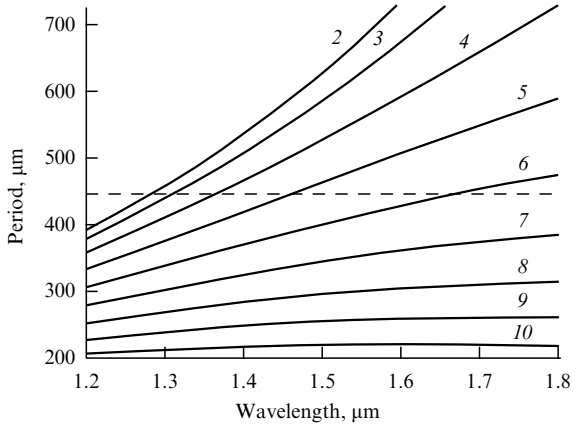

Figure 9. The grating period as a function of the resonance wavelength for cladding modes of various orders. Intersections of the curves with the horizontal dashed line determine the resonance wavelengths for a grating with a given period.

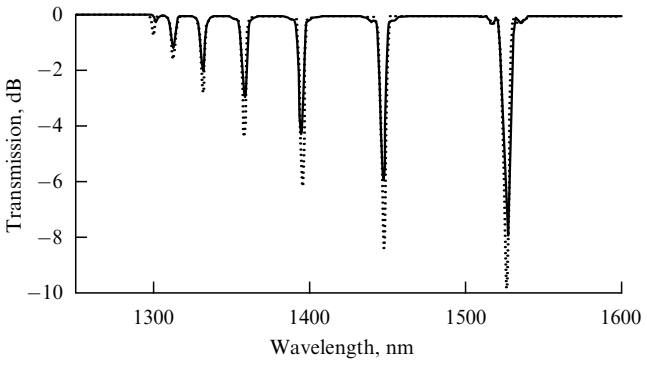

Figure 10. Experimental (solid line) and calculated (dotted line) transmission spectra of an LPFG with the period $\Lambda = 198$ nm and RI modulation $\Delta n = 3 \times 10^{-4}$ [34].

in the corresponding dips of the LPFG towards shorter wavelengths, i.e., oppositely to the shift of the resonances of cladding modes with small mode numbers [43].

The initial condition for measuring the transmission spectrum is that the amplitude of the cladding mode is equal to zero. Then, the transmission coefficient of an LPFG for a single cladding mode is given by

$$T = 1 - \frac{\kappa^2}{\eta^2} \sin^2 \eta L \,. \tag{45}$$

This function describes a dip with oscillations decaying on both of its sides (Fig. 11). The depth of the dip at the center is $\delta = 0$, and the minimum of transmission is achieved at $\kappa L = \pi/2$. The normalized spectral width of the dip is approximately given by the relation [3]

$$\frac{\Delta\lambda}{\lambda} = \frac{\lambda}{\Delta n_{\text{eff}} L} \sqrt{1 + \frac{4\kappa L}{\pi}}, \tag{46}$$

where $\Delta n_{\text{eff}} = n_{\text{eff}}^{\text{co}} - n_{\text{eff},m}^{\text{cl}}$. If the cladding mode is not lossless, which is always the case in practice, the shape of the resonance curve changes. The dip becomes somewhat broadened, and the side lobes are smoothed [44], which makes LPFGs more convenient for application in sensors and gain equalizers. Experimental spectra, are often not symmetric with respect to the resonance center. In Ref. [45], such an asymmetry is explained by the nonuniformity of the grating and the resulting inhomogeneity of $\Delta\beta^{\text{co}}$ along the grating.

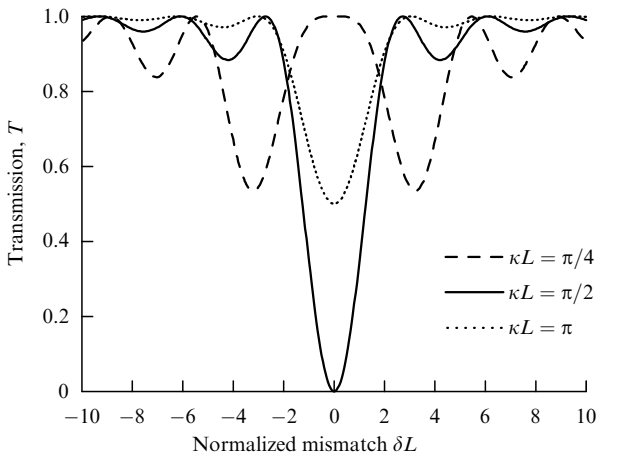

Figure 11. Transmission of an LPFG as a function of the normalized mismatch from the resonance for various products of the coupling coefficient and the grating length.

As the wavelength increases, the widths of the dips and the distance between them increase as well, due to both the increase in the wavelength and the resulting decrease in the ERI difference between the core and cladding modes, Δn_{eff}. Because of the sinusoidal factor $\sin^2 \kappa L$ in the grating transmission coefficient, the growth of the grating amplitude or its length may reduce the depths of dips corresponding to higher-order cladding modes in the transmission spectrum. This regime ($\kappa L > \pi/2$) is not used in LPFG-based devices because it leads to the suppression of the main resonance and the enhancement of additional maxima.

When a fiber with an LPFG is perturbed, the transmission spectrum of the LPFG is modified. First and foremost, the resonances change their positions. The wavelength shift of a resonance, $\Delta\lambda$, can be found from relation (42), which involves the propagation constants of two coupled modes and the grating period [46],

$$\Delta\lambda = -\frac{\Delta\beta^{\text{co}} - \Delta\beta_n^{\text{cl}} + 2\pi\Delta\Lambda/\Lambda}{\mathrm{d}\beta^{\text{co}}/\mathrm{d}\lambda - \mathrm{d}\beta_n^{\text{cl}}/\mathrm{d}\lambda} \,. \tag{47}$$

In a long-period fiber grating, much larger wavelength shifts can be obtained than in an FBG, for the same perturbation of the propagation constants. This is due to the extremely small denominator in Eqn (47), containing the difference $\mathrm{d}\beta^{\text{co}}/\mathrm{d}\lambda - \mathrm{d}\beta_n^{\text{cl}}/\mathrm{d}\lambda$. Exceptions are situations where identical perturbations are created both in the core and in the cladding of the fiber (for instance, due to stretching or heating) and, hence, $\Delta\beta^{\text{co}}$ and $\Delta\beta_n^{\text{cl}}$ almost cancel each other. The shifts observed in this case can be either larger or smaller than for FBGs [47].

Effective refractive indices of cladding modes have a strong dependence on the external radius of the cladding. Therefore, by changing the cladding radius, one can considerably change the positions of the resonances [48, 49]. The simplest way to change the radius of the fiber is chemical etching. However, this reduces the mechanical strength of the fiber and does not allow the positions of the resonances to be controlled in a dynamic way.

One can also control the positions of the resonances by doping the cladding with fluorine, Ba_2O_3 [50], or chromium ions, Cr^{3+}. Using these methods, it is possible to obtain LPFG spectra with a single resonance in a broad wavelength range. When germanium-doped fibers are kept in a hydrogen atmosphere in order to increase their photosensitivity, the positions of LPFG resonances may also change because hydrogen diffuses through the cladding and modifies the RI of the silica.

4.3 Fabrication methods

Because the period of an LPFG is much larger than that of an FBG, long-period fiber gratings are rather easy to produce, and there are many methods for fabricating them. All these methods are based on creating a periodic perturbation of the parameters of the fiber along its length (Fig. 12).

Historically, an LPFG was first produced by forming microbends of the fiber [5, 51]. In order to create a grating by means of this method, the fiber is fixed between two corrugated surfaces with grooves shifted by half the period

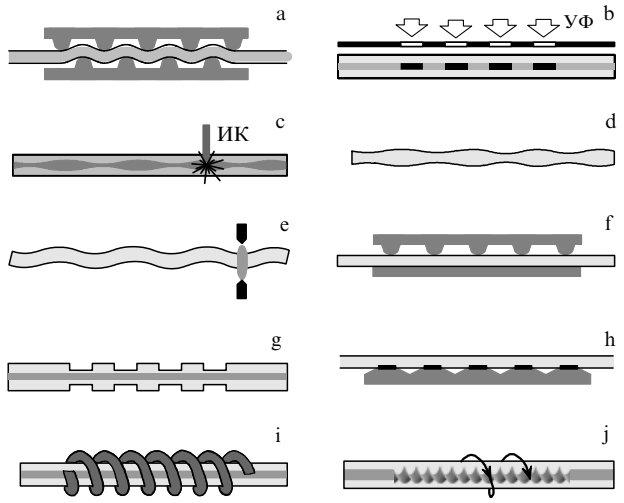

Figure 12. Methods of creating LPFGs: by microbending (a), photoinduction (b), IR irradiation (c), stretching (d), bending in an electric arc (e), pressing (f), etching (g), gluing to a substrate (h), winding (i), twisting (j).

(Fig. 12a). Gratings with microbends couple the core mode to the antisymmetric cladding modes LP_{1m}. In the first experiment, the dependence of the fiber transmission at a fixed wavelength on the period of microbends was studied; for certain periods of the grating, resonance energy losses were registered. Further, transmission spectra were measured with the grating period being fixed, and peaks of resonance losses were observed.

The most widely used method of creating LPFGs is based on photoinduction of gratings in germanosilicate fibers by UV laser pulses in the wavelength range 193 – 266 nm. Nonhomogeneous irradiation increases the RI in the illuminated parts of the core, which leads to a coupling between the core mode and the symmetric modes of the cladding. To enhance the photosensitivity of the fiber, it is kept, as in the case with FBG writing, in a hydrogen atmosphere. The gratings can be written point-by-point [52 – 54], using amplitude masks (Fig. 12b) [55, 56], holograms, microlenses [57], or reflecting amplitude masks [58]. Point-by-point writing allows obtaining gratings with an arbitrary structure along the fiber. Photo-induced LPFGs have a small birefringence, which reveals itself in the splitting of the resonances. The amplitudes and positions of loss peaks in LPFGs may change with time after the writing, which is a problem if a grating with given parameters is to be produced. To fit the positions of loss peaks, the cladding diameter is reduced by etching [48, 49, 59]. To reduce the wavelength shift of the peaks in the course of the gratings' photoinduction, the optical fiber can be preliminarily exposed to UV radiation [60].

To create long-period fiber gratings, the fiber can be irradiated by not only UV light but also visible or infrared light. The list of laser lines used for this purpose includes the 157 nm line of the F_2 laser [61], 193 nm [62] and 264 nm [63] lines of the ArF laser, the third harmonic of the neodimium laser and the 351 nm line of the Ar^+ laser, the second harmonic of the Ti: sapphire laser (400 nm) [64] or its fundamental harmonic (800 nm) [65], and the 10.6 μm line of the CO_2 laser [66 – 68]. The advantage of writing using a wavelength $\sim$ 355 nm rather than 248 nm is that in the former case, it is not necessary to remove the polymer coating, which means that the mechanical strength of the fiber is preserved [69]. Gratings produced with IR radiation have better stability at high temperatures. At the same time, such gratings have losses caused by fiber microdeformations and insufficient homogeneity [70]. Periodic laser heating of the fiber can be used for the diffusion of the doping agent from the core into the cladding (Fig. 12c) [71] or for creating microthinnings (Fig. 12d) [72, 73]. Poole et al. [74] produced microthinnings in a fiber by means of laser ablation and further annealing.

By heating a fiber in an electric arc, one can create microbends (Fig. 12e) [75] and remove stresses, which leads to the formation of an LPFG [76, 77]. A grating of periodic compression is formed when the fiber is pressed between two surfaces, a corrugated one and a flat one (Fig. 12f) [78, 79]. By removing parts of the fiber through chemical etching, one can form an etched LPBG (Fig. 12g) [46, 80 – 83]. When a stretching load is applied to such a grating, the etched parts undergo larger elastic deformations than the nonetched parts. This deformation modulation is converted, due to the photoelastic effect, into RI modulation. Similar effects take place when the etched structure is twisted or bent. A long-period fiber grating is also formed in an optical fiber glued to a periodically etched silicon substrate. The optical inhomogeneity of the fiber is caused in this case by the strains arising due to the hardening of polyamide adhesive (Fig. 12 h) [84]. LPFGs have also been created by the implantation of protons [85] and helium ions [86].

Helical deformations created in a fiber by winding a wire around it also form an LPFG (Fig. 12i) [87, 88]. A deformation of this kind couples the fundamental mode to a combination of four LP_{11} modes having various polarizations and profile orientations. Acousto-optical coupling between the core mode and the cladding modes occurs when an acoustic wave is excited in the fiber. This can be done by generating microbending waves in a fiber by means of a piezoelectric converter fixed to it; as a result, an antisymmetric LPFG is formed in the fiber [89]. The spectrum of such an LPFG can be controlled by means of a free parameter, which is the cladding radius; it can be reduced by stretching the fiber [90, 91].

Rego et al. [92] showed that etching can also be used for controlling the positions of peaks in the spectra of microbend gratings. In their experiment, microbend gratings were created with the help of corrugated rod. A fiber was placed against the rod, around both of which was wound a string, pressing the fiber into a groove in the rod. The strength of the resonances was controlled by varying the string tension.

Jeong et al. [93] induced an LPFG in a fiber with a capillary passing through its center and filled with a liquid crystal. The orientation of the liquid crystal director was set by electrodes periodically distributed along the fiber. In the absence of a bias field, the director was parallel to the capillary. When the field was applied, the director orientation in the sections between the electrodes was given by the field direction.

Recently, a new method of creating periodicity in a fiber was proposed, in which modes with different circular polarizations were distinguished [94]. A rectangular-core fiber was strongly twisted in a mini-oven. The resulting structure had a period of about 100 μm and the symmetry of a double helicoid (Fig. 12 j). Such a structure can be right- or left-handed. Each type of grating interacts only with modes of the corresponding circular polarization and transmits ortho-

gonally polarized modes without any changes. The twisting period determines the optical properties of the grating because the period enters the condition for the resonance between the core mode (with the corresponding polarization) and a cladding mode or, if the period is small, between the core mode and a radiation mode. Structures of this type are used as polarizers transmitting one polarization and dissipating the other.

4.4 Tilted gratings

Tilted LPFGs couple the fundamental mode of the core to the copropagating modes of the cladding with various radial and azimuthal numbers. The resonance condition is given by the relation $\beta^{co} + \Delta\beta^{co} - \beta_m^{cl} - \Delta\beta_m^{cl} = 2\pi \cos\theta/\Lambda$, where θ is the tilt angle of the grating. Calculations show that the coupling coefficients for s- and p-gratings have close values [16]. The effect of the tilt of an LPFG can be noticeable only at angles close to 90°. At the same time, the coupling coefficient for the HE_{1m} modes with $m < 17$ is much higher than the coupling coefficient for the corresponding EH_{1m} modes. The strongest coupling occurs for a certain radial mode number depending on the grating tilt angle, for instance, $\theta = 88°$ for $m = 8$. (Calculations were carried out for the same parameters of the fiber as in Section 3.3.) For modes with the azimuthal number 2, the situation is the opposite: the coupling coefficient for the EH_{2m} modes is much higher than for the HE_{2m} modes. Meanwhile, its maximal value is approximately 1.5 times less than the maximal coupling coefficient for the HE_{1m} modes. The maximal coupling coefficient for the HE_{3m} modes is 5 times smaller than the maximal coupling coefficient for the HE_{1m} modes. Modes with higher azimuthal numbers have negligibly small coupling coefficients.

Coupling coefficients for the HE_{1m} modes remain almost constant up to the tilt angle $\sim 87°$ and then dramatically decrease to zero at $\theta = 90°$ [16]. By contrast, for modes with higher azimuthal numbers ($v \geqslant 2$), the coupling coefficients are essentially nonzero only at tilt angles larger than 80°. The maximum coupling is achieved at tilt angles close to 88°. Thus, efficient coupling with higher-order cladding modes is possible at $\theta = 88°$. The exact value of the tilt angle at which the maximum is achieved depends on the radial mode number. It is worth noting that gratings of this kind, strictly speaking, cannot be considered long-period ones, because $\cos\theta$ becomes very small. For instance, for longitudinal period of the grating being 400 μm, the nominal period is 14 μm for a $\theta = 88°$ tilt and 7 μm for a $\theta = 89°$ tilt.

Tilted LPFGs can also be used for converting the core modes of few-mode optical fibers [17, 79]. If the fiber is rotated when a tilted grating is being written, a spiral grating is formed [95]. The resonance of such a grating is split into two peaks, the distance between them increasing as the twist period is reduced.

4.5 Long-period gratings in microstructured fibers

Similarly to FBGs, LPFGs can be created in microstructured fibers. Recently, several applications of such gratings were demonstrated: LPFG filters tunable in a broad range [32], LPFGs with thin-film heating elements [96], and LPFGs insensitive to external RI [29, 97].

A detailed study of LPFGs in MS fibers has been carried out in Refs [14, 29]. Long-period fiber gratings have been written in MS fibers by means of UV radiation at the wavelength 248 nm by scanning along the fiber through amplitude masks. To make the fiber photo-sensitive, a small germanium-doped core with the diameter ~ 1 μm and $\Delta = 5 \times 10^{-4}$ was formed in it. LPFGs were written in MS fibers of various types and transmission spectra were measured. The grating periods were chosen such that the resonance under study occurred at a wavelength near 1550 nm. In a PC fiber, an LPFG with the period 155 nm was written. Two resonances were observed in its spectrum, at wavelengths ~ 1050 nm and ~ 1600 nm. The second peak corresponded to a resonance with the fourth cladding mode, whose dip in the FBG spectrum (Fig. 8a) is denoted as 04. Placing the fiber into an immersion liquid led to practically no changes in the spectrum, which indicates that the cladding mode is guided by the holes of the PC fiber and its amplitude on the external boundary of the cladding is negligibly small. In contrast to LPFGs in ordinary fibers, long-period gratings in MS fibers are not sensitive to the RI of the surrounding medium [3, 7].

The small effective diameter of the 'grapefruit' fiber inner cladding can be used for the development of tunable LPFG filters whose central wavelength can be tuned within a broader range than that typical for LPFG filters written in ordinary fibers. A broader tuning range for the resonance wavelength is achieved due to the larger distance between the peaks of the cladding modes, which is inversely proportional to the cladding diameter. Filling the holes of the MS fiber with a polymer whose RI has a strong temperature dependence also leads to an increase the tuning range. In experiments of this type, an acrylic polymer with an RI close to that of fused silica was introduced into the air holes of a 'grapefruit' fiber [32] and then cured under UV radiation. An LPFG with the period 550 μm was induced in the fiber through an amplitude mask. The grating provided a cladding resonance at the wavelength ~ 1550 nm for the mode denoted as 02 in Fig. 8b. For this grating, the tuning range was over 150 nm, which much exceeded the tuning ranges of ordinary DPFGs.

Measurements of the LPFG spectra in 'air-ring' fibers, both in the air and in an immersion liquid, show that such LPFGs are almost insensitive to the RI of the surrounding medium [97]. If the air holes are filled with a polymer, these LPFGs can also be tuned by heating within a broader range than LPFGs in ordinary fibers [96].

Creation of an LPFG in an MS fiber does not necessarily require a photosensitive core. In an MS fiber without a doped core, an LPFG can be induced by periodic compression of the fiber [98, 99], an acoustic microbending wave [100], collapse of the holes due to fiber heating by CO_2 laser radiation [101, 102], or electric arc [103]. It should be mentioned that a polymer PC fiber was used in Ref. [98]. For gratings induced through microcompressions and microbendings, both the amplitude and the resonance wavelength of the grating can be controlled. The amplitude can be controlled by varying the pressure or the acoustic wave amplitude, while to control the resonance wavelength, one can change the grating period by variation of the angle between the fiber and the plate grooves or variation of the acoustic wave frequency. Lim et al. [99] described an unusual behavior of LPFGs in PC fibers, where the resonance wavelength was shifted towards the shortwave side of the spectrum with increase in the grating period, whereas in ordinary fibers, the shift is towards the longwave range.

Long-period fiber gratings obtained by means of an electric arc, which causes the collapse of the holes in a PC fiber, have very high temperature stability up to 1200 °C. The resonance wavelength shift observed in such gratings due to

heating is six times smaller than the shift in an ordinary LPFG. Using a CO_2 laser, Zhu et al. [102] formed in a PC fiber an ultra-short grating having only 8 periods with the total length 2.8 mm. Collapse of the holes reduced the fiber diameter to 101 nm. The obtained grating had a 31 dB absorption peak; however, in a broad region around the resonance, the losses exceeded 10 – 15 dB, which made this grating not very suitable for practical applications.

An interesting way to control resonance LPFGs in a 'grapefruit' MS fiber was suggested by Mach et al. [104]. A microstructured fiber with a written LPFG is partly filled by two liquids, one of them having an RI larger than that of the silica cladding and the other one smaller than the cladding RI. Then, this fiber is spliced between two ordinary single-mode fibers. If a temperature difference is created between the ends of the MS fiber, then the air pressure makes the two liquids move with respect to the LPFG. Thus, the cladding mode is propagating through a fiber in which one part is filled by a liquid with an RI higher than that of the silica and the other part by a liquid with an RI lower than that of the silica. The considerable difference between the type of propagation of various cladding modes allows tuning the LPFG transmission spectrum.

4.6 Nonlinear effects in long-period gratings

High-speed fiber-optical communications of the future require the creation of simple, compact devices based on all-optical signal processing, i.e., devices where light is controlled by light only. This means that nonlinear-optical elements are needed. The most important nonlinearities are the second-order and third-order ones. For instance, the second-order nonlinearity of potassium dihydrophosphate (KDP) is successfully used in bulk-crystal systems for signal processing, pulse compression, and soliton propagation. However, standard optical fibers are center-symmetric and hence manifest no quadratic nonlinear effects. Therefore, studies in fiber optics are focused on weaker third-order nonlinear phenomena [105], which consist of the RI dependence on the light wave intensity,

$$n = n_0 + n_2 I\,, \tag{48}$$

where n_0 is the linear RI, I the light wave intensity, and n_2 the nonlinear RI, which, in the case of silica and the wavelength 1500 nm, is equal to 2.6×10^{-16} cm^2 W^{-1}.

It is especially interesting to study nonlinear effects in periodic fiber structures such as Bragg and long-period gratings. Nonlinear effects in LPFGs were first observed in birefringent fibers with a periodically rocking anisotropy axis (rocking filters) [106]. In a structure of this kind, a mode of a certain polarization is converted into a mode of orthogonal polarization. For the modes to be resonantly coupled, the anisotropy axis rocking period must coincide with the beat length. As the intensity of light propagating through the fiber increases, the nonlinear variation of the fiber RI changes the beat length and leads to the dependence of the inter-mode conversion efficiency on the light intensity.

The two copropagating modes can be the core mode and a cladding mode. The nonlinearity of an LPFG can bring the modes into resonance or from resonance, due to the variation of the intensity-dependent RI. To control the resonance in LPFGs, much smaller intensities are required than in the case of Bragg gratings [107 – 109]. The reason, as we already mentioned in Section 4.2, is that even small variations of the RI lead to a considerable shift in the LPFG resonance wavelength. In addition, in contrast to the case of Bragg gratings, the influence of the material dispersion on the properties of LPFGs is negligibly small due to the small difference between the ERIs of the core and the cladding. Similarly to the linear case, nonlinear propagation of a pulse in an LPFG can be described by the coupled-mode equations [110], which, in general, can be solved only numerically:

$$\begin{aligned}
&\frac{\partial A^{\mathrm{co}}}{\partial z} + \beta^{\mathrm{co}\prime}\,\frac{\partial A^{\mathrm{co}}}{\partial t} = \mathrm{i}\kappa^{\mathrm{co-co}} A^{\mathrm{co}} + \mathrm{i}\,\frac{M}{2}\,k_m^{\mathrm{co-cl}} \exp\left(-\mathrm{i}2\delta z\right) \\
&+ \mathrm{i}\left(\Gamma^{\mathrm{co-co}}\left|A^{\mathrm{co}}\right|^2 + 2\Gamma_m^{\mathrm{co-cl}}\left|A_m^{\mathrm{cl}}\right|^2\right) A^{\mathrm{co}}\,, \\
&\frac{\partial A_m^{\mathrm{cl}}}{\partial z} + \beta_m^{\mathrm{cl}\prime}\,\frac{\partial A_m^{\mathrm{cl}}}{\partial T} = \mathrm{i}\kappa_m^{\mathrm{cl-cl}} A^{\mathrm{cl}} + \mathrm{i}\,\frac{M}{2}\,\kappa_m^{\mathrm{cl-co}} A^{\mathrm{co}} \exp\left(\mathrm{i}2\delta z\right) \\
&+ \mathrm{i}\left(2\Gamma_m^{\mathrm{co-cl}}\left|A^{\mathrm{co}}\right|^2 + \Gamma_m^{\mathrm{cl-cl}}\left|A_m^{\mathrm{cl}}\right|^2\right) A_m^{\mathrm{cl}}\,,
\end{aligned} \tag{49}$$

where $\Gamma_{pq} = 3/16\,\omega\varepsilon_0\chi^{(3)}\int |\mathbf{E}_p|^2|\mathbf{E}_q|^2\,\mathrm{d}S$ are nonlinear coupling coefficients, $\beta_p' = \partial\beta_p/\partial\omega$ are inverse group velocities, the indices p and q correspond to either the core mode or the mth cladding mode, and $\chi^{(3)}$ is the third-order nonlinear susceptibility.

Equations (49) were analyzed numerically for a 50-mm-long LPFG and a 70 ps Gaussian pulse fed into the core [108]. The RI modulation amplitude in the LPFG was chosen such that in the linear regime at the center of the resonance, the core mode would be fully converted into a cladding mode. Figure 13 shows the evolution of the pulse shape in the core (Fig. 13a, c, e) and the cladding (Fig. 13b, d, f) of an optical fiber at the detuning corresponding to the first side maximum of the LPFG spectrum, $\delta = 150$ m^{-1} and the initial intensity $I_0 = 20$ GW cm^{-2} (Fig. 13a, b), $\delta = 150$ m^{-1} and $I_0 = 25$ GW cm^{-2} (Fig. 13c, d), and the center of the spectrum, $\delta = 0$ and $I_0 = 12$ GW cm^{-2} (Fig. 13e, f). From Fig. 13a, b, one can see that the pulse wings, which have small intensity, are mismatched with the resonance and weakly interact with the cladding mode, while the pulse peak is in resonance with the cladding mode, its energy being efficiently converted into the cladding mode, such that a single-peak pulse is formed in the cladding. If the intensity of the pulse increases, the shift becomes larger than the mismatch, and the peak exits from the resonance. This case is shown in Figs 13c, d, where the pulse peak has a weak coupling with the cladding mode. For intermediate intensities, nonlinearity brings the core and cladding modes back into resonance, and the pulse in the cladding takes a double-peak shape. Thus, the initial intensity of the pulse determines its shape at the output from the LPFG. Figure 13e, f shows the case where the mismatch is zero and low-intensity pulse wings are at resonance, while the pulse peak is detuned from the resonance because of the nonlinearity. This effect creates a doubly peaked pulse propagating through the cladding; in other words, it is possible to split a pulse into several shorter pulses. Comparison of the numerical simulation results with the experimental data demonstrated their good agreement [108]. To vary the mismatch with the resonance, the fiber was heated, which shifted the center of the LPFG spectrum.

An alternative theoretical analysis of nonlinear pulse propagation in LPFGs was carried out by Jeong et al. [109], who used the coupled-mode discrete theory and considered a more general case of coupling with several cladding modes due to a nonsinusoidal distribution of the RI along the fiber. The possibility of pulse compression was demonstrated.

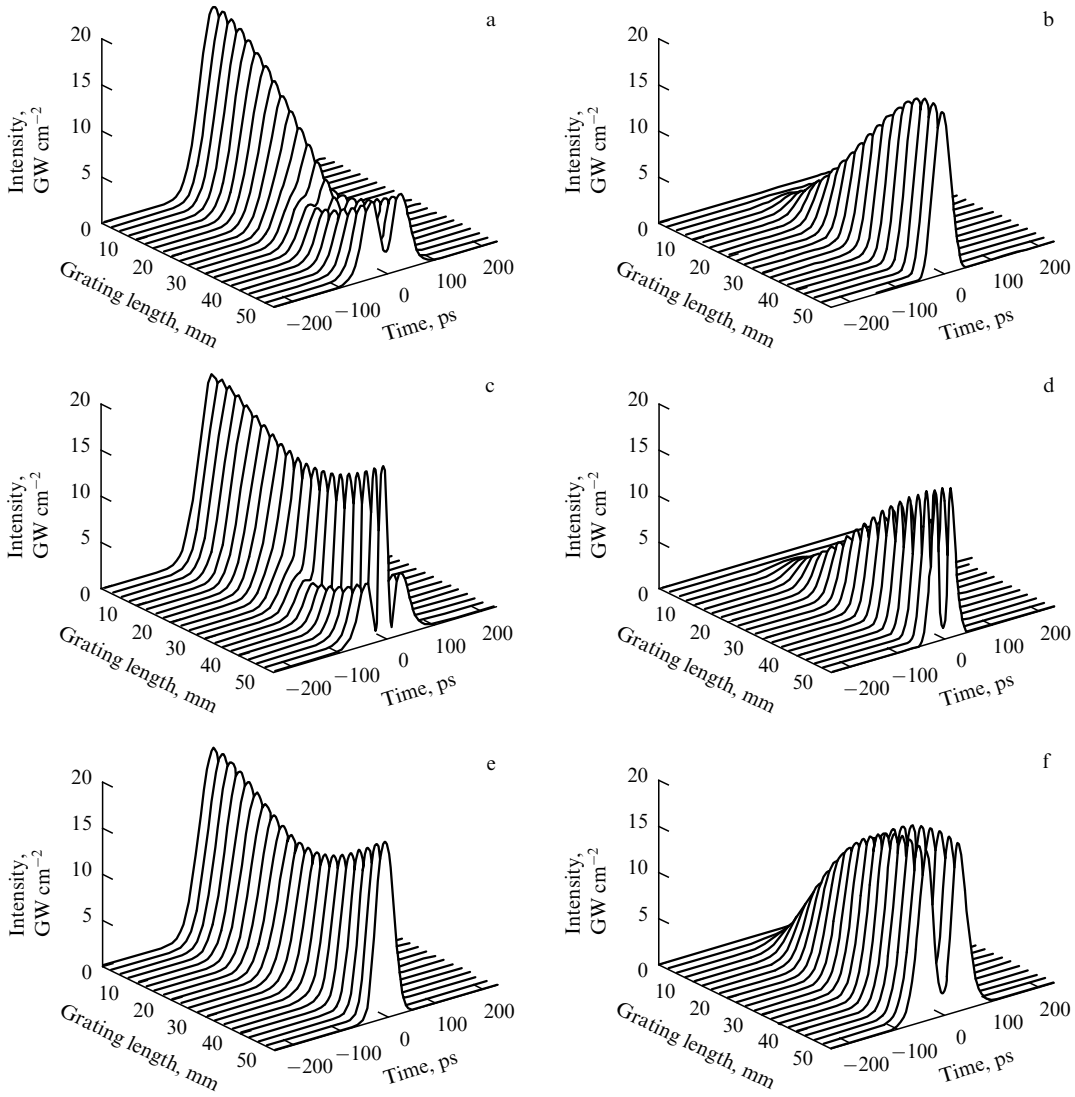

Figure 13. Evolution of the shape of a pulse passing through an LPFG, in the core (a, c, e) and the cladding (b, d, f) for the detuning $\delta = 150$ m^{-1} and intensity $I_0 = 20$ GW cm^{-2} (a, b); $\delta = 150$ m^{-1} and $I_0 = 25$ Gw cm^{-2} (c, d); $\delta = 0$ and $I_0 = 12$ GW cm^{-2}(e, f) [108].

The nonlinear effects described above can be observed at intensities about 10 GW cm^{-2}, which are far too high for application in telecommunication lines. High intensities are required because the length at which the modes interact is of the order of only several centimeters. For this reason, Perlin et al. [111] proposed a new scheme of a longer grating, based on cascaded LPFGs, which requires intensities two orders of magnitude smaller than in the case of a usual LPFG. The idea is to increase the distance along which the interacting modes propagate. For this, a piece of ordinary fiber of length D is inserted into the grating, such that a cascaded grating is formed, which consists of two parts with lengths αL and $(1 - \alpha) L$, separated by the distance D. While propagating through the fiber between the gratings, the pulse accumulates a sufficiently large nonlinear phase shift. However, in this case, the pulses propagating along the core and the cladding have different velocities and arrive at the end of the grating at different moments of time. To compensate for this effect, a mirror-symmetric cascade grating consisting of parts with lengths $(1 - \alpha) L$ and αL is placed at the distance $2D$ from the end of the first structure. The resulting length of the grating is $4D + 2L$.

A scheme with a cascaded LPFG was also used for the measurement of the optical nonlinearities of fibers doped with ytterbium and aluminum ions [112]. A nonlinear RI at the signal mode wavelength ($\lambda = 1550$ nm) was shown to depend on the intensity of the pump (at the wavelength 96 nm) and to be 7.5×10^{-15} m^2 W^{-1}. According to the Kramers–Kronig relation, the change in the RI is caused by the decrease in the absorption of ytterbium ions caused by the pump. This nonlinear effect was used for the experimental demonstration of all-optical switching in a cascaded LPFG [113, 114] within the frequency range 1– 250 Hz with the extinction coefficient ~ 18 dB for the pump power 35 mW. The signal mode is transmitted or not transmitted through the cascade LPFG depending on the pump intensity. A similar principle allows the signal to be switched between two fiber channels [115]. However, in this case, it is impossible to observe the whole variety of nonlinear phenomena because the RI variation is observed at a wavelength different from the pump wavelength.

The coupled-mode method has been used in Refs [116, 117] to study the conditions for the formation and propagation of soliton pulses in optical fibers with LPFGs. Coupled-

mode equations were reduced to equations for partial pulses with the dispersion and nonlinearity given by some effective parameters. Based on these equations, modulation instability of a wave packet propagating in an LPFG was studied [117]. It was shown that modulation instability could exist in the range of normal material dispersion of the fiber.

The nonlinear optical properties of LPFGs can be analyzed not only via the standard coupled-mode theory but also using the transfer-matrix method [118]. For rectangular pulses, this method has shown that nonlinear propagation through an LPFG is equivalent to linear propagation through a chirped grating.

Nonlinear interaction between the core mode and a cladding mode can be used for passive mode locking in a fiber laser [119]. For this, an LPFG is written in a fiber, such that a low-intensity signal is resonantly coupled to one of the cladding modes. At higher intensities, the resonance condition is violated. As a result, for a pulse passing through the grating, the weak wings are converted into a cladding mode and the pulse center, being nonresonant, propagates further as a core mode.

4.7 Polarization effects in long-period gratings

The RI changes induced in a germanium-doped fiber core under exposure to UV radiation, similarly to the RI changes in mechanically induced LPFGs or other types of gratings, is generally asymmetric with respect to the fiber axis [120, 121]. This asymmetry reveals itself in the birefringence of fiber modes, i.e., in the dependence of the mode ERI on their polarization, and may be useful in designing polarization fiber-optical elements. But in some cases, birefringence can be harmful and its influence should be reduced. In any case, polarization effects in LPFGs should be investigated because they have a considerable effect on the parameters of the gratings.

An efficient way to enhance polarization effects in LPFGs is to write the gratings in strongly birefringent fibers [122 – 125]. Transmission spectra of LPFGs in birefringent fibers contain absorption peaks that are split into two. The splitting is caused by the fact that the phase matching conditions for orthogonally polarized modes are different, which, in turn, is because orthogonally polarized modes in a birefringent fiber have different propagation constants. For fibers with asymmetric cladding, polarization splitting can be caused by the polarization properties of the cladding modes [123].

In addition, the maximal RI modulation amplitudes are different for different polarization states. A change in the modulation amplitude leads to different coupling and transmission coefficients for differently polarized modes. Thus, modes of each polarization have their own resonance wavelengths and amplitudes [126].

If the transmitted radiation is polarized along one of the birefringence axes, the spectrum contains a corresponding cladding resonance peak. Therefore, LPFGs with large resonance splitting can be used as polarization filters [125]. The resonance splitting can vary from several nanometers up to 40 nm in fibers with asymmetric cladding.

The dependence of losses on the polarization direction has been used for the precise local measurement of birefringence in optical fibers [127]. The accuracy of birefringence measurement was $\sim 10^{-8}$, which is two orders of magnitude better than the accuracy of other methods. An erbium laser was created based on an LPFG used as a polarization filter [128]. The light emitted by this laser is linearly polarized, with the polarization degree being being as high as 98%. Polarization effects caused in LPFGs by fiber twisting and the application of a magnetic field have been studied in Refs [129, 4].

An important task is to eliminate polarization dependence of losses in the fiber-optical elements whose properties should be as little polarization-dependent as possible [71, 130, 121].

4.8 Applications of long-period fiber gratings

Long-period fiber gratings find applications in various fiber-optical devices. In particular, LPFGs are used in radiation sources for equalizing their spectra, in elements with tunable spectral characteristics, for dispersion control, and for group-velocity dispersion compensation. Based on LPFGs, fiber interferometers and multi-wavelength lasers are created.

Amplifiers based on erbium-doped fibers (EDFs) are widely used in communication systems with WDM. However, the gain of such amplifiers has a nonuniform wavelength distribution. To equalize the gain spectrum, LPFG-based filters are used, their advantages being compactness, simplicity of fabrication, small loss, and extremely low intensity of the reflected signal [131 – 136]. To equalize the gain spectrum of an EDF-based amplifier, it is necessary to use a filter with the absorption spectrum inverted with respect to the gain peak at the wavelength 1530 nm. This way, the gain peak is flattened (Fig. 14).

Because LPFGs are used as spectrum equalizers, an important practical problem is to develop LPFGs with a given transmission spectrum. This requires solving an inverse problem. For calculating the RI distribution along the fiber grating from a given transmission spectrum, methods based on solving the Gelfand – Levitan – Marchenko integral equations have been developed [137]. The main drawback of these methods is the difficulty of solving the integral equations in the general case. Iteration methods based on solving the Gelfand – Levitan – Marchenko integral equations converge slowly and have low algorithmic efficiency, because they require $O(N^3)$ operations, where N is the number of intervals in the grating.

There are methods based on optimization algorithms minimizing the discrepancy between the initial spectrum and the spectrum of the calculated grating. Variation optimiza-

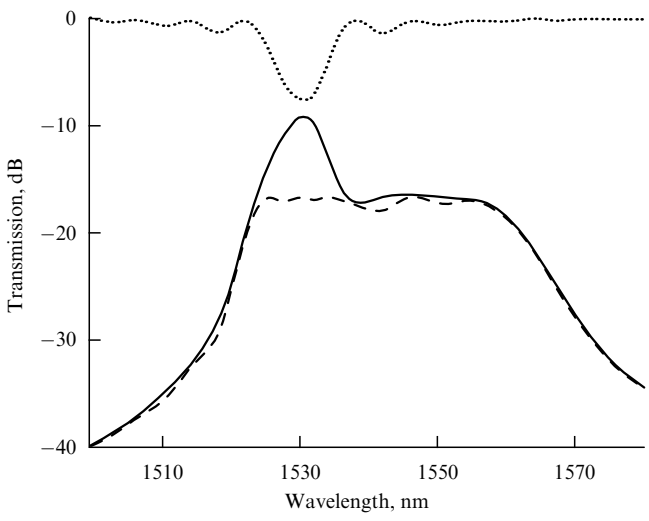

Figure 14. Initial gain spectrum of an EDF-based amplifier (solid line), the LPFG spectrum (dotted line), and the final amplifier spectrum after gain equalization (dashed line) [133].

tions and genetic algorithms are described in the literature. However, these methods have even slower convergence.

The most efficient are differential methods, which take full advantage of the layered structure of the grating in which the wave propagates. These methods, based on the causality principle, restore the parameters of the medium layer-by-layer. The algorithmic efficiency of such methods is high because the number of operations they require depends quadratically on the number of intervals in the structure, $O(N^2)$. The first differential algorithm developed was the one for reconstructing the coupling coefficient profile in an FBG in the case of coupling between counter-propagating modes [138]. This algorithm, called the layer peeling method, was later generalized to the case of coupling between copropagating modes in an LPFG [139].

An important problem for integrating optoelectronic devices into fiber-optical systems is radiation coupling into and out of a single-mode fiber. An efficient way to reduce losses in this case is to use cladding modes instead of the core mode, which has a larger divergence angle [140 – 143]. Using cladding modes for radiation input and output considerably reduces the requirements for the structure geometry, which otherwise are too strict.

The following LPFG-based schemes have been proposed for the input/output of radiation: the fiber – fiber system where LPFGs are written in both fibers (Fig. 15a) [140]; the fiber – fiber system (Fig. 15b) in which the transmitting fiber radiates the core mode into free space and the receiving fiber has a lens tip transforming the free-space beam into a cladding mode, which is further converted by an LPFG into the core mode of the receiving fiber; the diode – fiber system (Fig. 15c) [142, 143], and the fiber – free space system (Fig. 15d) [141]. For an optical fiber, the input/output can be based on the surface coupling of the modes propagating in joined parallel waveguides (Fig. 15e) [144 – 147].

As we have mentioned, LPFGs are sensitive to various factors influencing the optical fiber where the grating is formed. This enables one to create, first, LPFG-based devices with tunable spectral properties and, second, sensors of various physical parameters.

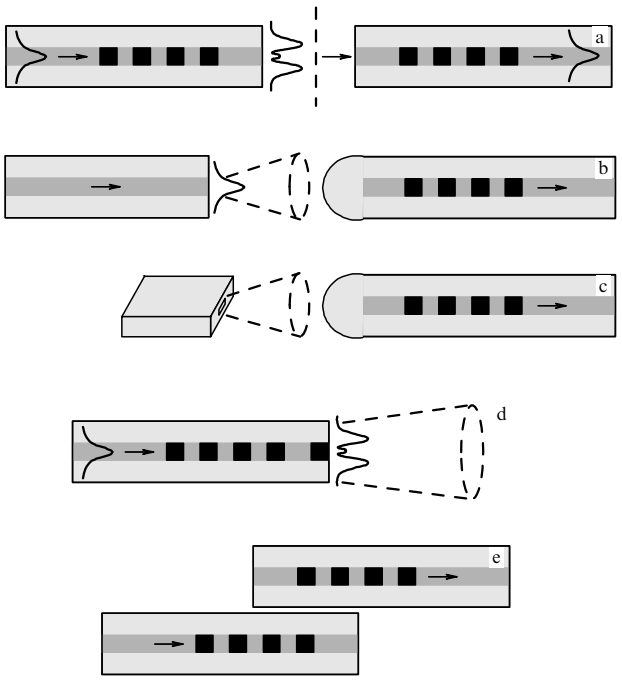

Figure 15. Schemes for fiber input and output of radiation using cladding modes and LPFGs.

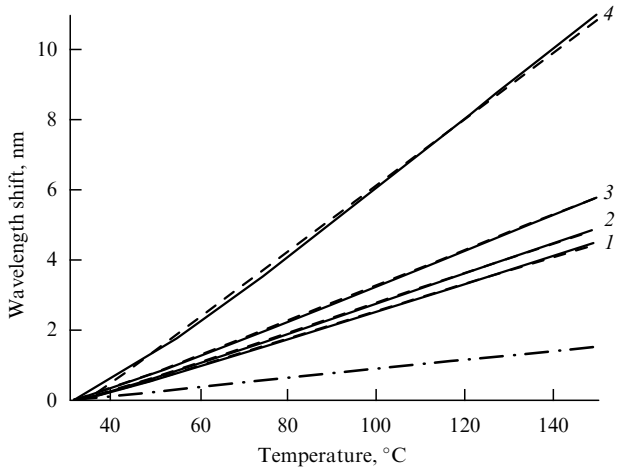

Figure 16. Shift in the resonance wavelengths of cladding modes caused by the change in the LPFG temperature: the experimental data (solid curves), linear approximation (dashed lines), and corresponding shift of a Bragg grating resonance (dashed-dotted line) [47].

Variation of the LPFG temperature leads to a shift in its resonance wavelength [148 – 151]. The value of the shift depends on the mode number, wavelength, and grating period and may be positive or negative [47, 55]. Figure 16 shows the temperature dependences of shifts for four cladding resonances of a photo-induced LPFG (solid curves), their linear approximations (dashed lines), and, for comparison, the analogous shift for the peak of a Bragg grating (dashed-dotted line).

Similarly to the temperature variation, stretching also leads to a shift in the LPFG resonance wavelength [47, 55, 91]. In ordinary fibers, the shift is up to 2 nm $\mu\varepsilon^{-1}$ ($\mu\varepsilon$, the microstrain, is a dimensionless quantity characterizing relative deformation, $1\,\mu\varepsilon = 10^{-6}$ cm cm^{-1}). In etched gratings, longitudinal stretching does not shift resonance peaks but only changes their heights [80 – 82]. If a transverse stress is applied to the LPFG, the fiber becomes birefringent; as a result, each resonance is split into two, corresponding to orthogonal polarization states [152]. A shift is also observed in the case of twisting [46, 67, 153 – 155], but its value depends quadratically on the twist angle. An example of such a dependence is given in Fig. 17, where symbols denote experimental values and curves are fitting parabolas. The bending of an LPFG causes three kinds of responses: a shift of the central wavelength, a change in the resonance amplitude, and the resonance band splitting.

Microbend LPFGs are easily tunable: the grating strength is determined by the amplitude of the microbends and the grating period can be varied by varying the angle between the fiber and the grooves of the plates between which the fiber is pressed [153].

Because the cladding modes are guided by the external cladding of the fiber, which is in contact with the surrounding medium, propagation of cladding modes depends on the parameters of the medium, such as the refractive index and absorption coefficient [149, 157, 158]. The amplitude and phase of the wave reflected at the boundary between the cladding and the surrounding medium depends on the

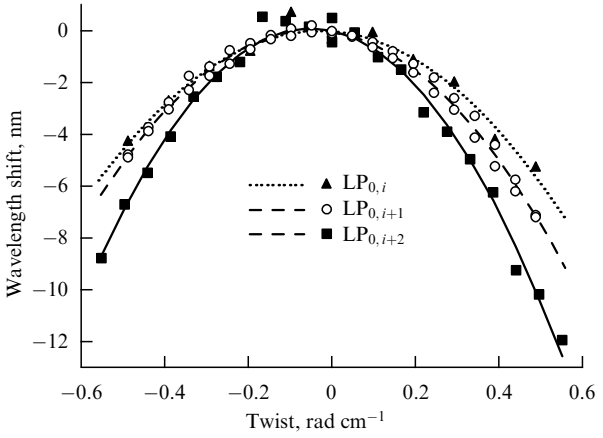

Figure 17. Shift in the resonance wavelengths of cladding modes due to the twisting of LPFGs: experimental results (symbols) and parabolic fitting curves [46].

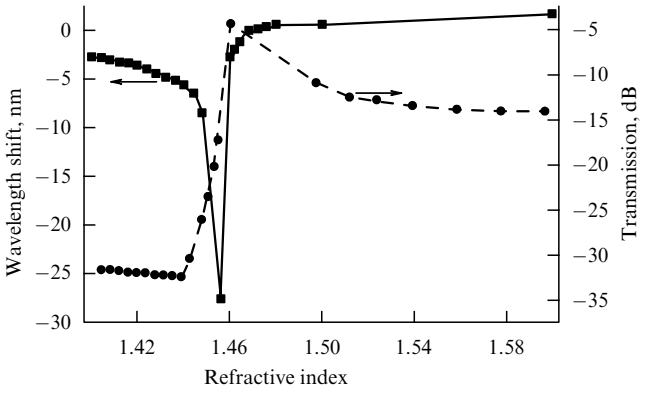

Figure 18. Shift in the resonance wavelength of a cladding mode and variation of the depth of the corresponding peak in the transmission spectrum due to the RI variation of the surrounding medium [149].

parameters of the surrounding medium, and therefore a change in these parameters leads to a change in the ERI and losses for the cladding modes. This, in its turn, modifies the resonance condition and shifts the resonance wavelength [47, 73] or changes the height of the loss peak [149] (Fig. 18).

In LPFG spectra, several absorption peaks are observed. External influences change both the shapes and positions of the peaks. The way a peak is modified depends on the type of external influence (variation of the temperature, strain, RI of the surrounding medium, etc.). One can make a separate measurement to find the response of the LPFG to the variation of any certain parameter; then, it is possible to solve the inverse problem and to calculate the necessary parameters from the measured changes in the spectrum. This way, it is possible to make multi-parameter sensors for the simultaneous measurement of several parameters [159].

A detailed list of references on LPFG-based sensors can be found in review [160].

4.9 Cascaded gratings

An optical-fiber interferometer based on two successive LPFGs was first proposed by Dianov et al. [161, 162]. Its operation is illustrated in Fig. 19. In the first grating, the core mode converts half of its energy into the cladding mode. Next, both modes propagate along the fiber with slightly different

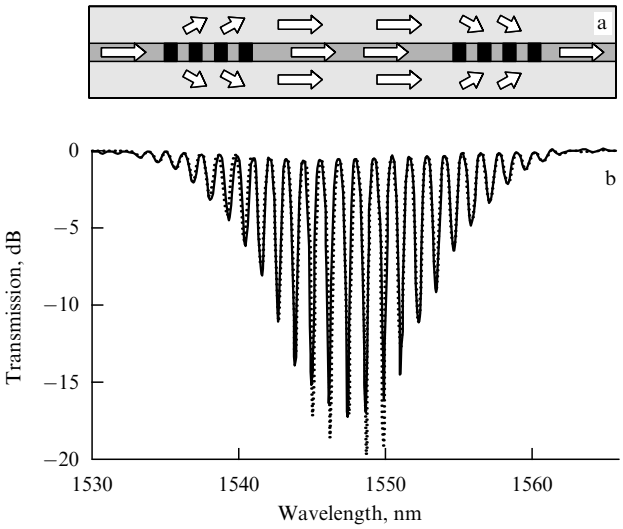

Figure 19. Propagation of radiation in a cascaded LPFG (a) and its transmission spectrum (b) [164]. Solid line shows the experimental results and the dotted line shows the calculated spectrum.

velocities and reach the second grating, which couples them again (Fig. 19a).

The spectrum of a cascaded LPFG has a comb-like shape with multiple peaks, whose envelope coincides with the transmission spectrum of a single LPFG (Fig. 19b). The wavelength difference for the neighboring peaks is determined by the distance between the two LPFGs in the cascade and is about one or several nanometers.

Because the spectrum of a cascaded LPFG consists of narrow peaks, this structure is very sensitive to various factors [124, 163]. Indeed, cascaded LPFGs have been used for measuring photo-induced changes in the fiber RI under UV radiation [162] and CO_2-laser pulses [165]. A change in the RI can be measured with a high accuracy through the measurement of interference fringes shift. Cascaded LPFGs have also been used as sensors of the temperature [166], longitudinal [167] and transverse [169, 170] strains, bending [168, 169], and refractive index of the external medium [169, 170, 172].

Recently, cascaded LPFGs with microbends were created in PC fibers [99]. The transmission spectra of such LPFGs manifest interference fringes, similar to the fringes of a cascade grating in a standard fiber but with somewhat less regular structure. Ramachandran et al. [173] proposed a bandpass filter based on a cascaded grating. Losses in cascaded gratings can show considerable polarization dependence due to the small width of the resonance peaks [174, 175].

Cascaded LPFGs are used to study optical nonlinearity in fibers as well as for all-optical switching. A piece of EDF is placed between two LPFGs. Radiation at the wavelength 976 nm makes the transmission spectrum of the cascade grating shift due to the RI dependence on the light wave intensity [112, 176]. As the interference pattern shifts by half the period, the regime of transmission at a certain wavelength switches to the regime of nontransmission [113].

Because of the comb-like structure of their spectra, cascaded LPFGs are used in the fabrication of multi-wavelength radiation sources, which are required in WDM systems [177 – 180].

Another example of a system consisting of several uniform LPFGs is a structure with a series of successive LPFGs

phase-shifted with respect to each other [133, 181 – 185]. The phase shift is created by a uniform piece of fiber, unexposed to UV radiation and having the length equal to several fractions of the LPFG period, placed between two gratings.

In addition to the above-described gratings, other combined structures have been studied, containing an LPFG and a mirror, a cascaded LPFG with core-mode blocking, a combination of a short-period grating and a long-period one, multiple LPFGs, two FBGs, chirped LPFGs, and LPFGs with modulation of the amplitude, grating period, fiber parameters, and microbending modulation.

5. Conclusion

In this review, we have considered various questions related to the existence of special modes in optical fibers, namely, those propagating in the cladding.

Exact and approximate methods of calculating the field distribution profiles for cladding modes have been presented. The exact calculation is based on the matrix method, in which the fiber is divided into uniform coaxial layers, and each layer is described by the corresponding 4×4 matrix. The matrix of the whole structure is found as the product of the matrices for separate layers. The problem is solved by finding the eigenvalues and eigenvectors of this matrix.

In the paraxial approximation, the solution for low-order cladding modes can also be found for gradient fibers. Although the refractive index perturbation in the core is quite small, the core has considerable influence on the distribution profiles of the cladding modes.

If the cladding has a coating with the refractive index exceeding that of fused silica, cladding modes become leaky. For such a mode, losses can be described by introducing the imaginary part of the propagation constant. Another way of solving this problem is to consider the radiation modes of the fiber.

The transmission spectrum of an FBG contains not only the Bragg peak but also a group of peaks shifted towards the shortwave range. These peaks correspond to reflection into the cladding modes. If the cladding has a coating with a higher refractive index, resonance peaks of the cladding modes are smoothed. They disappear completely if the refractive index of the coating is equal to the refractive index of the cladding.

In photoinduced FBGs and LPFGs, coupling with the core mode is different for the HE and EH cladding modes. The coupling coefficients for the HE modes are considerably higher than the coupling coefficients for the corresponding EH modes with radial mode numbers below 10. The reason is that the fields of EH modes have small amplitudes near the core, where the grating is recorded. Tilted FBGs and LPFGs couple the core mode to the cladding modes with arbitrary azimuthal numbers, and not only with $v = 1$, as in the case of nontilted gratings. To provide high coefficients of reflection into low-order cladding modes, the tilt angle of a Bragg grating should not exceed several degrees.

An important problem is the suppression of cladding resonances in Bragg gratings. For this purpose, the refractive index profile is chosen such that the overlap integrals for the core and cladding modes are minimized. In addition, the photosensitivity profile can be expanded to the cladding area, where the core mode amplitude decays exponentially.

Cladding modes are most widely used in LPFGs that couple copropagating modes. In the transmission spectra of such LPFGs, there are broad dips (with widths as large as dozens of nanometers) caused by energy coupling from the core mode into cladding modes. About ten different methods of fabricating LPFGs have been proposed, all of them consisting of a periodic perturbation of the optical fiber. Long-period gratings can be tilted, similarly to the Bragg gratings, but the tilt angle should not differ from 90° by more than several degrees for the tilt effect to be noticeable.

Resonances of the cladding modes can also be observed for Bragg and long-period gratings written in MS fibers. Long-period gratings written in MS fibers allow obtaining effects that are not possible in the case of standard fibers.

In long-period fiber gratings, the third-order nonlinearity can lead to the effects of pulse reshaping, including pulse compression. In a cascaded LPFG, the possibility of all-optical switching has been demonstrated. Polarization effects lead to the splitting of cladding-mode resonances, which can be used for fabricating polarization filters and for the precise measurement of birefringence in optical fibers.

In order to use LPFGs as gain equalizers for fiber radiation sources, special methods have been developed for solving the inverse problem of calculating the refractive index distribution along the fiber grating from a given transmission spectrum. One of the most efficient is the layer peeling method.

When cladding modes exit from the cladding into free space, their divergence is much smaller than the divergence of the core mode in a single-mode fiber. Therefore, cladding modes can be used for radiation input and output.

In contrast to the core modes, cladding modes are sensitive to the refraction index of the surrounding medium and can therefore be used in refractive-index sensors. Other sensors based on cladding modes have been proposed, measuring temperature, longitudinal stress, transverse pressure, bending, twisting, microbends, and other physical parameters. Based on measurements of several cladding peaks or measuring several parameters of the spectrum, multi-parameter sensors can be constructed.

LPFGs are used in complex cascaded structures containing several gratings. The loss spectrum of a cascaded LPFG grating consists of multiple closely spooned peaks, the distances between them being determined by the length of the fiber between the two gratings. Because of this, cascaded LPFGs can be used for the design of multi-wavelength radiation sources.

The presented results of the research on cladding modes and components based on their existence in optical fibers demonstrate the broad possibilities for their application in fiber-optical devices and for the control of radiation, as well as in various sensors.

List of abbreviations

FBG — fiber Bragg grating
LPFG — long-period fiber grating
RI — refractive index
ERI — effective refractive index
MS — microstructure
WDM — wavelength division multiplexing
PC — photonic crystal
EDF — erbium-doped fiber

References

1. Tsao C *Optical Fibre Waveguide Analysis* (Oxford: Oxford Univ. Press, 1992)
2. Kaliteevskiĭ M A, Nikolaev V V, Abram R A *Opt. Spektrosk.* **88** 871 (2000) [*Opt. Spectrosc.* **88** 792 (2000)]
3. Erdogan T *J. Opt. Soc. Am. A* **14** 1760 (1997); "Errata" *J. Opt. Soc. Am A* **17** 2113 (2000)
4. Ivanov O V *J. Opt. Soc. Am. A* **22** 716 (2005)
5. Bjarklev A *J. Lightwave Technol.* **4** 341 (1986)
6. Vasil'ev S A et al. *Kvantovaya Elektron.* **26** 65 (1999) [*Quantum Electron.* **29** 65 (1999)]
7. Erdogan T *J. Lightwave Technol.* **15** 1277 (1997)
8. Hou R et al. *Meas. Sci. Technol.* **12** 1709 (2001)
9. Duhem O et al. *Appl. Opt.* **37** 7223 (1998)
10. Koyamada Y *J. Lightwave Technol.* **18** 1220 (2000)
11. Stegall D B, Erdogan T *Photon. Technol. Lett.* **11** 343 (1999)
12. Dong L, Reekie L, Cruz J L *Electron. Lett.* **33** 1897 (1997)
13. Poladian L, Issa N, Monro T *Opt. Express* **10** 449 (2002)
14. Eggleton B J et al. *J. Lightwave Technol.* **18** 1084 (2000)
15. Kerbage C et al. *Opt. Express* **7** 113 (2000)
16. Lee K S, Erdogan T *Appl. Opt.* **39** 1394 (2000)
17. Lee K S, Erdogan T *J. Opt. Soc. Am. A* **18** 1176 (2001)
18. Dong L, Ortega B, Reekie L *Appl. Opt.* **37** 5099 (1998)
19. Laffont G, Ferdinand P *Meas. Sci. Technol.* **12** 765 (2001)
20. Baek S, Jeong Y, Lee B *Appl. Opt.* **41** 631 (2002)
21. Haggans C W et al. *Photon. Technol. Lett.* **10** 690 (1998)
22. Dong L et al. *Photon. Technol. Lett.* **9** 64 (1997)
23. Zhang L et al. *Opt. Lett.* **23** 1665 (1998)
24. Dong L et al. *J. Lightwave Technol.* **18** 1583 (2000)
25. Parker R, de Sterke C M *J. Lightwave Technol.* **18** 2133 (2000)
26. Haggans C W et al. *J. Lightwave Technol.* **16** 902 (1998)
27. Kim J M et al. *Photon. Technol. Lett.* **12** 1504 (2000)
28. Eggleton B J et al. *IEEE J. Sel. Top. Quantum Electron.* **7** 409 (2001)
29. Eggleton B J et al. *Opt. Lett.* **24** 1460 (1999)
30. Zheltikov A M *Optika Mikrostrukturirovannykh Volokon* (Optics of Microstructure Fibers) (Moscow: Nauka, 2004)
31. Zheltikov A M *Usp. Fiz. Nauk* **170** 1203 (2000) [*Phys. Usp.* **43** 1125 (2000)]
32. Westbrook P S et al. *Photon. Technol. Lett.* **12** 495 (2000)
33. Vasil'ev S A et al. *Kvantovaya Elektron.* **24** 151 (1997) [*Quantum Electron.* **27** 146 (1997)]
34. Zhao Y, Palais J C *J. Lightwave Technol.* **16** 554 (1998)
35. Yamada M, Sakuda K *Appl. Opt.* **26** 3474 (1987)
36. Chern G W, Wang L A *J. Opt. Soc. Am. A* **16** 2675 (1999)
37. Ke H, Peng J, Fan C *Photon. Technol. Lett.* **13** 1194 (2001)
38. Murtaza G et al. *Fiber Integr. Opt.* **20** 53 (2001)
39. Shu X, Huang D *Opt. Commun.* **171** 65 (1999)
40. Ramachandran S, Wang Zh, Yan M *Opt. Lett.* **27** 698 (2002)
41. Han Y-G et al. *Photon. Technol. Lett.* **13** 699 (2001)
42. Grubsky V, Feinberg J *Opt. Lett.* **25** 203 (2000)
43. MacDougall T W et al. *Photon. Technol. Lett.* **10** 1449 (1998)
44. Daxhelet X, Kulishov M *Opt. Lett.* **28** 686 (2003)
45. Eom T-J et al. *IEICE Trans. Commun. E Ser. B* **E-84B** 1241 (2001)
46. Ivanov O V, Wang L A *Appl. Opt.* **42** 2264 (2003)
47. Bhatia V *Opt. Express* **4** 457 (1999)
48. Vasiliev S A et al. *Opt. Lett.* **21** 1830 (1996)
49. Zhou K, Liu H, Hu X *Opt. Commun.* **197** 295 (2001); "Erratum" *Opt. Commun.* **208** 433 (2002)
50. Oh K, Song G H, Paek U C, in *CLEO/Pacific Rim'99*: *the Pacific Rim Conf. on Lasers and Electro-Optics, August 30 – September 3, 1999, Seoul, Korea, Technical Digest* (Piscataway, NJ: IEEE, 1999) paper ThB6, p. 601
51. Marcuse D *Appl. Opt.* **23** 1082 (1984)
52. Dianov E M et al. *Opt. Lett.* **22** 221 (1997)
53. Dianov E M et al. *Kvantovaya Elektron.* **24** 160 (1997) [*Quantum Electron.* **27** 155 (1997)]
54. Hill K O et al. *Electron. Lett.* **26** 1270 (1990)
55. Vengsarkar A M et al. *J. Lightwave Technol.* **14** 58 (1996)
56. Bhatia V, Vengsarkar A M *Opt. Lett.* **21** 692 (1996)
57. Liu S Y, Tan H Y, Demokan M S *Electron. Lett.* **35** 79 (1999)
58. Patrick H J et al. *Electron. Lett.* **33** 1167 (1997)
59. Kim S et al. *Appl. Opt.* **39** 2038 (2000)
60. Kawano H et al. *J. Lightwave Technol.* **19** 1221 (2001)
61. Chen K P et al. *Opt. Lett.* **26** 771 (2001)
62. Guan B-O et al. *Meas. Sci. Technol.* **12** 818 (2001)
63. Kryukov P G et al. *Microelectron. Eng.* **69** 248 (2003)
64. Zagorul'ko K A et al. *Kvantovaya Elektron.* **31** 999 (2001) [*Quantum Electron.* **31** 999 (2001)]
65. Kondo Y et al. *Opt. Lett.* **24** 646 (1999)
66. Rao Y J et al. *Opt. Commun.* **229** 209 (2004)
67. Rao Y-J et al. *J. Lightwave Technol.* **21** 1320 (2003)
68. Kim B H et al. *Opt. Lett.* **26** 1657 (2001)
69. Starodubov D S, Grubsky V, Feinberg J *Proc. SPIE* **3848** 178 (1999)
70. Vasiliev S A, Medvedkov O I *Proc. SPIE* **4083** 212 (2000)
71. Dianov E M et al., in *ECOC'97*: *23rd European Conf. on Optical Communication, September 22 – 25, 1997, Edinburg, UK* Vol. 2 (IEE Conf. Publ., No. 448) (Piscataway, NJ: IEEE, 1997) p. 53
72. Kakarantzas G et al. *Opt. Lett.* **26** 1137 (2001)
73. Chong J H et al. *Opt. Commun.* **229** 65 (2004)
74. Poole C D, Presby H M, Meester J P *Electron. Lett.* **30** 1437 (1994)
75. Hwang I K, Yun S H, Kim B Y *Opt. Lett.* **24** 1263 (1999)
76. Rego G et al. *J. Lightwave Technol.* **19** 1574 (2001)
77. Kosinski S G, Vengsarkar A M, in *OFC'98*: *Optical Fiber Communication Conf. and Exhibit: Technical Digest*: *February 22 – 27, 1998, San Jose, Calif., USA* (OSA Technical Digest Ser., Vol. 2) (Washington, DC: Optical Society of America, 1998) p. 278
78. Cho J Y, Lee K S *Opt. Commun.* **213** 281 (2002)
79. Lee K S, Cho J Y *J. Opt. Soc. Am. A* **19** 1621 (2002)
80. Vaziri M, Chen C-L *J. Lightwave Technol.* **15** 474 (1997)
81. Vaziri M, Chen C-L *J. Lightwave Technol.* **10** 836 (1992)
82. Lin C-Y, Wang L A, Chern G-W *J. Lightwave Technol.* **19** 1159 (2001)
83. Lin C-Y, Chern G-W, Wang L A *J. Lightwave Technol.* **19** 1212 (2001)
84. Jiang Y et al. *Photon. Technol. Lett.* **14** 941 (2002)
85. Fujimaki M et al. *Opt. Lett.* **25** 88 (2000)
86. von Bibra M L, Roberts A, Canning J *Opt. Lett.* **26** 765 (2001)
87. Poole C, Townsend C, Nelson K *J. Lightwave Technol.* **9** 598 (1991)
88. Berthold J W *J. Lightwave Technol.* **13** 1193 (1995)
89. Kim H S et al. *Photon. Technol. Lett.* **10** 790 (1998)
90. Feced R et al. *IEEE J. Select. Topics Quantum Electron.* **5** 1278 (1999)
91. Diez A et al. *Electron. Lett.* **36** 1187 (2000)
92. Rego G et al. *Opt. Commun.* **220** 111 (2003)
93. Jeong Y et al. *Photon. Technol. Lett.* **12** 519 (2000)
94. Kopp V I et al. *Science* **305** 74 (2004)
95. Lee K S *Opt. Commun.* **198** 317 (2001)
96. Abramov A A et al. *Photon. Technol. Lett.* **11** 445 (1999)
97. Espindola R P et al. *Electron. Lett.* **35** 327 (1999)
98. van Eijkelenborg M A, Padden W, Besley J A *Opt. Commun.* **236** 75 (2004)
99. Lim J H et al. *Opt. Lett.* **29** 331 (2004)
100. Diez A et al. *Opt. Lett.* **25** 1499 (2000)
101. Kakarantzas G, Birks T A, Russell P St J *Opt. Lett.* **27** 1013 (2002)
102. Zhu Y et al. *Opt. Lett.* **28** 2467 (2003)
103. Humbert G et al. *Opt. Lett.* **29** 38 (2004)
104. Mach P et al. *Appl. Phys. Lett.* **80** 4294 (2002)
105. Kivshar Yu S, Agrawal G P *Optical Solitons*: *from Fibers to Photonic Crystals* (Amsterdam: Academic Press, 2003) [Translated into Russian (Moscow: Fizmatlit, 2005)]
106. Trillo S et al. *Appl. Phys. Lett.* **53** 837 (1988)
107. Eggleton B J et al. *Opt. Lett.* **22** 883 (1997)
108. Kutz J N et al. *IEEE J. Select. Topics Quantum Electron.* **3** 1232 (1997)
109. Jeong Y, Lee B *IEEE J. Quantum Electron.* **35** 1284 (1999)
110. Sipe J E, DeSterke C M, Eggleton B J *J. Mod. Opt.* **49** 1437 (2002)
111. Perlin V E, Winful H G *J. Lightwave Technol.* **18** 329 (2000)
112. Kim Y H et al. *Opt. Lett.* **27** 580 (2002)
113. Kim Y et al. *Opt. Express* **12** 651 (2004)
114. Kim Y H, Paek U-C, Han W-T *J. Lightwave Technol.* **23** 543 (2005)
115. Kim Y H, Paek U-C, Han W-T *Appl. Opt.* **44** 3051 (2005)
116. Zolotovskiĭ I O, Sementsov D I *Opt. Spektrosk.* **92** 306 (2002) [*Opt. Spectrosc.* **92** 272 (2002)]
117. Zolotovskiĭ I O, Sementsov D I *Kvantovaya Elektron.* **31** 50 (2001) [*Quantum Electron.* **31** 50 (2001)]

118. Chern G-W, Chang J-F, Wang L A *J. Opt. Soc. Am. B* **19** 1497 (2002)
119. Intrachat K, Kutz J N *IEEE J. Quantum Electron.* **39** 1572 (2003)
120. Bachim B L, Gaylord T K *Appl. Opt.* **42** 6816 (2003)
121. Oh S et al. *Opt. Express* **11** 3087 (2003)
122. Lin C-H, Li Q, Lee H P *Opt. Lett.* **28** 998 (2003)
123. Kurkov A S et al. *Electron. Lett.* **33** 616 (1997)
124. Zhang L et al. *IEEE J. Select. Topics Quantum Electron.* **5** 1373 (1999)
125. Ortega B et al. *Photon. Technol. Lett.* **9** 1370 (1997)
126. Ryu H S et al. *Opt. Lett.* **28** 155 (2003)
127. Ishii Y et al., in *OFC 2002*: *Optical Fiber Communication Conf. and Exhibit, March 17–22, 2002, Anaheim, CA, USA* (OSA Trends in Optics and Photonics, Vol. 70) (Washington, DC: Optical Society of America, 2002) p. 686
128. Kurkov A S et al. *Kvantovaya Elektron.* **31** 421 (2001) [*Quantum Electron.* **31** 421 (2001)]
129. Arce-Diego J L, Pereda-Cubián D, Muriel M A *J. Opt. A*: *Pure Appl. Opt.* **6** S45 (2004)
130. Kim S Y et al., in *Conf. on Lasers and Electro-Optics* (*CLEO 2000*): *May 7–12, 2000, San Francisco, CA, USA* (Trends in Optics and Photonics Ser., Vol. 39) (Washington, DC: Optical Society of America, 2000) p. 576
131. Vengsarkar A M et al. *Opt. Lett.* **21** 336 (1996)
132. Guan B-O et al. *Photon. Technol. Lett.* **14** 657 (2002)
133. Liu Y et al. *Opt. Commun.* **164** 27 (1999)
134. Harumoto M, Shigehara M, Suganuma H *J. Lightwave Technol.* **20** 1027 (2002)
135. Su C D, Wang L A *J. Lightwave Technol.* **17** 1896 (1999)
136. Ramachandran S et al. *Photon. Technol. Lett.* **15** 1561 (2003)
137. Chern G-W, Wang L A *J. Opt. Soc. Am. A* **19** 772 (2002)
138. Feced R, Zervas M N, Muriel M A *IEEE J. Quantum Electron.* **35** 1105 (1999)
139. Feced R, Zervas M N *J. Opt. Soc. Am. A* **17** 1573 (2000)
140. Li Y, Erdogan T *Opt. Commun.* **183** 377 (2000)
141. Erdogan T et al., in *OFC/IOOC'99*: *Optical Fiber Communication Conf. and the Intern. Conf. on Integrated Optics and Optical Fiber Communication, February 21–26, 1999, San Diego, CA, USA* (OSA Technical Digest Ser.) (Washington, DC: Optical Society of America, 1999) paper FK4
142. Su W-Y, Chern G-W, Wang L A *Appl. Opt.* **41** 6576 (2002)
143. Chen W T, Wang L A *Appl. Opt.* **39** 4490 (2000)
144. Chiang K S et al. *Electron. Lett.* **36** 1408 (2000)
145. Chiang K S, Chan F Y M, Ng M N *J. Lightwave Technol.* **22** 1358 (2004)
146. Zhu Y et al. *Opt. Commun.* **208** 337 (2002)
147. Grubsky V, Starodubov D S, Feinberg J, in *Optical Fiber Communication Conf., March 7–10, 2000, Baltimore, Maryland, USA* (OSA Trends in Optics and Photonics, Vol. 37) (Washington, DC: Optical Society of America, 2000) paper FB5
148. Ivanov O V *Opt. Commun.* **239** 311 (2004)
149. Khaliq S, James S W, Tatam R P *Meas. Sci. Technol.* **13** 792 (2002)
150. Shu X et al. *Photon. Technol. Lett.* **13** 818 (2001)
151. Jang J-N et al. *Electron. Lett.* **35** 2134 (1999)
152. Liu Y, Zhang L, Bennion I *Electron. Lett.* **35** 661 (1999)
153. Ivanov O V *Opt. Commun.* **232** 159 (2004)
154. Gonzalez D A, in *Proc. of Second European Workshop on Optical Fiber Sensors, Santander, Spain, June 9–11, 2004* (Proc. SPIE, Vol. 5502) (Bellingham, WA: SPIE, 2004)
155. Wang L A, Lin C Y, Chern G W *Meas. Sci. Technol.* **12** 793 (2001)
156. Liu Y, Williams J A R, Bennion I *Photon. Technol. Lett.* **12** 531 (2000)
157. Chung K-W, Yin S *Opt. Lett.* **29** 812 (2004)
158. Wang Z, Ramachandran S *Opt. Lett.* **28** 2458 (2003)
159. Patrick H J et al. *Photon. Technol. Lett.* **8** 1223 (1996)
160. James S W, Tatam R P *Meas. Sci. Technol.* **14** R49 (2003)
161. Dianov E M et al., in *22nd European Conf. on Optical Communication, ECOC'96, Oslo, Norway, September 15–19, 1996* (Piscataway, NJ: IEEE, 1996) MoB.3.6, p. 65
162. Dianov E M et al. *Kvantovaya Elektron.* **24** 805 (1997) [*Quantum Electron.* **27** 785 (1997)]
163. Das M, Thyagarajan K *Opt. Commun.* **197** 67 (2001)
164. Lee B H, Nishii J *Appl. Opt.* **38** 3450 (1999)
165. Kim B H et al. *Appl. Opt.* **41** 3809 (2002)
166. Kim Y-J, Paek U-C, Lee B H *Opt. Lett.* **27** 1297 (2002)
167. Han Y-G et al. *Opt. Express* **11** 476 (2003)
168. Lee B H, Nishii J *Opt. Lett.* **23** 1624 (1998)
169. Han Y-G et al. *Meas. Sci. Technol.* **12** 778 (2001)
170. Duhem O, Henninot J F, Douay M *Opt. Commun.* **180** 255 (2000)
171. Lee B H et al. *Fiber Integr. Opt.* **20** 443 (2001)
172. Lee S et al., in *Proc. of the OECC/IOOC 2001, 1–5 July 2001, Sydney, Australia,* p. 112
173. Ramachandran S et al. *Opt. Lett.* **27** 1678 (2002)
174. Lee B H, Cheong J, Paek U-C *Opt. Lett.* **27** 1096 (2002)
175. Lee Y W, Jung J, Lee B *Photon. Technol. Lett.* **14** 1312 (2002)
176. Jeong Y, Baek S, Lee B *Photon. Technol. Lett.* **12** 1216 (2000)
177. Han Y-G et al. *Photon. Technol. Lett.* **15** 383 (2003)
178. Gu X J *Opt. Lett.* **23** 509 (1998)
179. Lee J H et al., in *OECC 2002, 7th Optoelectronics and Communications Conf., Yokohama, Japan, July 2002,* 10P-46, p. 278
180. Lee J H et al., in *Proc. of COIN 2002*: *Intern. Conf. on Optical Internet, Korea, July 2002*, WeE1, p. 300
181. Deparis O et al. *Opt. Lett.* **26** 1239 (2001)
182. Chen L R *Opt. Commun.* **200** 187 (2001)
183. Chen L R *Opt. Commun.* **205** 271 (2002)
184. Ke H, Chiang K S, Peng J H *Photon. Technol. Lett.* **10** 1596 (1998)
185. Ishii Y et al., in *ECOC'01, 27th European Conf. on Optical Communication*: *September 30–October 4, 2001, Amsterdam, The Netherlands* (Piscataway, NJ: IEEE, 2001) Mo.B.3.4. p. 82